AD612197

FIREBALL PHENOMENOLOGY

Harold L. Brode

October 1964

COPY 2 OF 3
HARD COPY $.3.00
MICROFICHE $.0.50
51p

DDC
ARCHIVED
MAR 19 1965
DDC-IRA E

P-3026

ARCHIVE COPY

FIREBALL PHENOMENOLOGY

Harold L. Brode*

The RAND Corporation, Santa Monica, California

*Any views expressed in this paper are those of the author. They should not be interpreted as reflecting the views of The RAND Corporation or the official opinion or policy of any of its government or private research sponsors. Papers are reproduced by The RAND Corporation as a courtesy to members of its staff.

This paper was prepared for presentation at The Tripartite Technical Cooperation Panel Meeting, Panel N3, held at the Joint Fire Service College, Dorking, England, 5-9 October 1964. The papers are to be published by Defense Atomic Support Agency.

FIREBALL PHENOMENOLOGY

This paper deals with some of the properties of nuclear explosions which influence the predictions and scalings for fireball phenomena, notably fireball sizes, temperatures, densities, and ultimately the thermal radiation output. Attention is focused on the initial features of fireball formation for which we shall examine the scaling with both yield and altitude of burst. For the present, these scalings are derived from a few theoretical calculations which describe fireball features for several yields and altitudes. In the near future more calculations of comparable and greater precision promise to provide more exact scaling laws.

The yields and the energy densities for modern weapons range over many orders of magnitude. The yields may range from fractions of a kiloton to tens or even hundreds of thousands of kilotons, i.e., into the 100 megaton range. These enormous ranges of energies are not matched by comparable ranges in the mass required in the weapons, so that the yield-to-mass ratio may likely change by quite large fractions. Thus we can expect that the energy density or the mean temperatures of the bomb vapors at the time of the release of nuclear energy may have a comparably wide range. Typically the exterior of a weapon may reach peak temperatures of tens of millions of degrees centigrade.

Since all of the energies of a nuclear explosion are generated in an extremely short time (small fractions of a microsecond) and within a small mass and volume, the properties of that small mass and volume (the weapon itself and its immediate surroundings) dominate the early fireball phenomena and even influence the character of the later thermal radiation.

The initial radiations from a nuclear weapon (i.e., the gamma rays and neutrons, and the x-ray radiations from the extremely high temperatures of the bomb vapors) are largely determined by the bomb materials and the construction of the nuclear weapon itself and are not determined by the external environment. Thus, whether the explosion takes place in the atmosphere, out in space, underwater, or underground does not matter much in the achievement of the initial energy densities and radiative properties. Such is not strictly true in every environment, but, provided the immediate surroundings are not as dense as the weapon itself, the fraction of energy which may be radiated out as x-rays before the bomb itself begins to blow apart under hydrodynamic action depends only upon its yield-to-mass ratio and its construction detail. This fraction may range from almost nothing at all (or a very small per cent) to significantly more than 80% of the total energy generated.

The energy which does escape as x-rays in this early phase does not escape far from atmospheric explosions, because x-rays in this range of a few tens of million degrees kelvin are x-rays of a rather "soft" nature. X-rays of one or two kilovolts energy have mean free paths in air which are quite short; consequently, they are absorbed in the air immediately around the bomb. However, as the air around the bomb is heated to very high temperatures it becomes less absorbent. That is, the air atoms become hotter and their absorption properties become those of a completely ionized plasma in which the x-rays are treated to Compton scatterings only. Thus, the hot air becomes relatively transparent to x-rays as they come streaming out of the bomb vapors, and the cold air remains quite opaque.

In this way, the earliest stages can be characterized rather simply by an extremely high temperature sphere of air surrounding the source and showing a fairly sharp temperature drop at its edge. The interior of this high temperature sphere may be at a fairly uniform temperature, and it may contain quite a large fraction of the nuclear explosion energy. With this simplification or approximation, one can view the early phases of nuclear explosions as independent of the details of the weapon design. This is true to

the extent that a large fraction of the energy is very early contained in the air and, therefore, the properties of this air will determine the subsequent explosion behavior.

The Table below indicates that relatively small spheres of air contain quite large amounts of energy at the high temperatures which are created by these x-ray emmanations. These temperatures, of course, are too high for the air to remain that hot for very long, but in the immediate first fractions of a microsecond these radii are representative of the size and temperatures of the earliest (x-ray) fireball.

SIZE OF SPHERES OF SEA LEVEL AIR NECESSARY TO CONTAIN 1 KT, 1 MT OR 100 MT OF ENERGY AT VARIOUS UNIFORM TEMPERATURES

Temperature Millions of ^{o}C	Radius For Hot Air Sphere		
	1 KT	1 MT	100 MT
7½	3/4 m	7.5 m	35 m
6	1	10	46
5	1¼	12	57
4	1.6	16	74
3	2.1	21	100

In the next few microseconds this air re-radiates very rapidly into the cold air, and the fireball grows by a radiation diffusion process.

In Fig. 1 we see a typical temperature and density profile at an early time (34 μs) in which the temperatures within the hot sphere are relatively uniform but exhibit a sharp outer edge. In the same figure the density curve shows relatively little change from the ambient condition outside of the weapon itself. In fact, there is only a slight compression at the front of the fireball and a slight rarefaction, or reduction in density, in the interior. Figure 1 further shows a high compression or shock within the bomb materials, which, at this time of 34 microseconds, have expanded out to some

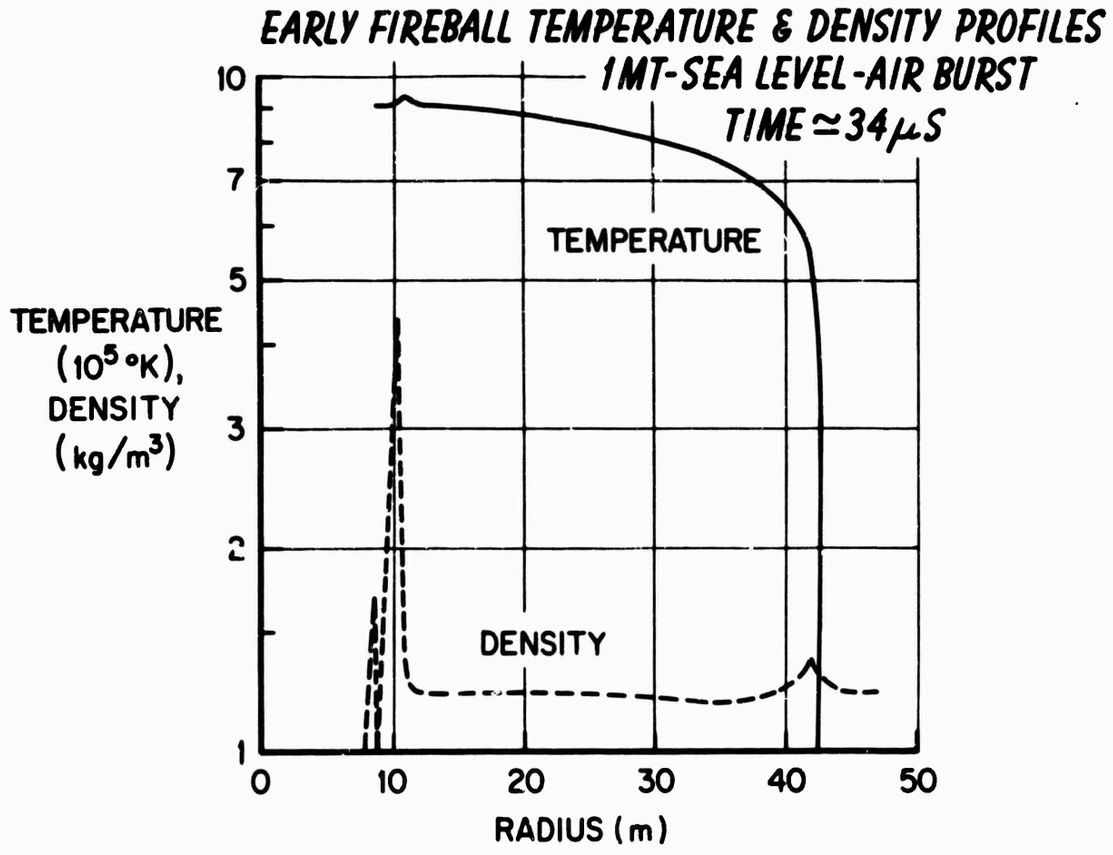
EARLY FIREBALL TEMPERATURE & DENSITY PROFILES
1MT-SEA LEVEL-AIR BURST
TIME ≃ 34μS
TEMPERATURE
DENSITY
TEMPERATURE (10^5 °K), DENSITY (kg/m^3)
10
7
5
3
2
1
0
10
20
30
40
50
RADIUS (m)

Fig. 1

ten meters. This shock has blown all the vapors out into a relatively high density shell around a xtremely low density interior. Note that the temperature is highest at the bomb surface, where the material is also most dense, but that the temperatures are not markedly different anywhere while the densities are.

Figure 2 illustrates the distribution of pressure and of velocity at this same time (34 μs) for this one megaton sea level example. The pressures show a similar profile to those of the temperatures within the hot air and further show the shock wave that is associated with the expanded bomb vapors. Similarly, the bomb vapors are seen to be expanding at an extremely high velocity, while the air is just beginning to move out in the rest of the fireball. Of course, as the bomb vapors expand they pick up the air and compress it highly in this non-adiabatic, nearly isothermal, interior shock

Figure 3 illustrates, on a logarithmic plot, the dependence of the various fronts on radius and time. The radiation front itself is seen to expand at the earliest fractions of a microsecond to tens of meters, slowing down markedly as the energy from the bomb is depleted and the energies remaining in the bomb are no longer allowed to radiate out because of the increasing opacity of the vapors as their temperatures drop. At the same times, one sees the bomb itself expanding in what is labelled as the case shock. Ultimately, the bomb vapors drop behind as more and more air is picked up and this shock moves away. The case shock then chases out through the hot fireball as the fireball itself begins also to shock up at its outer surface forming a more normal, strong, adiabatic shock.

Each of these features - the radiation expansion front, the transition to a shock front at that fireball front, the expansion of the bomb vapors, and the generation of the case shock - may be expected to scale differently for different weapons, for different yields, and for different altitudes of burst. If the design of the weapon allowed less radiation out or more radiation to remain in the case, then the point of intersection of these two shocks would surely be changed, although the yield of the explosion and the altitude of burst may be the same.

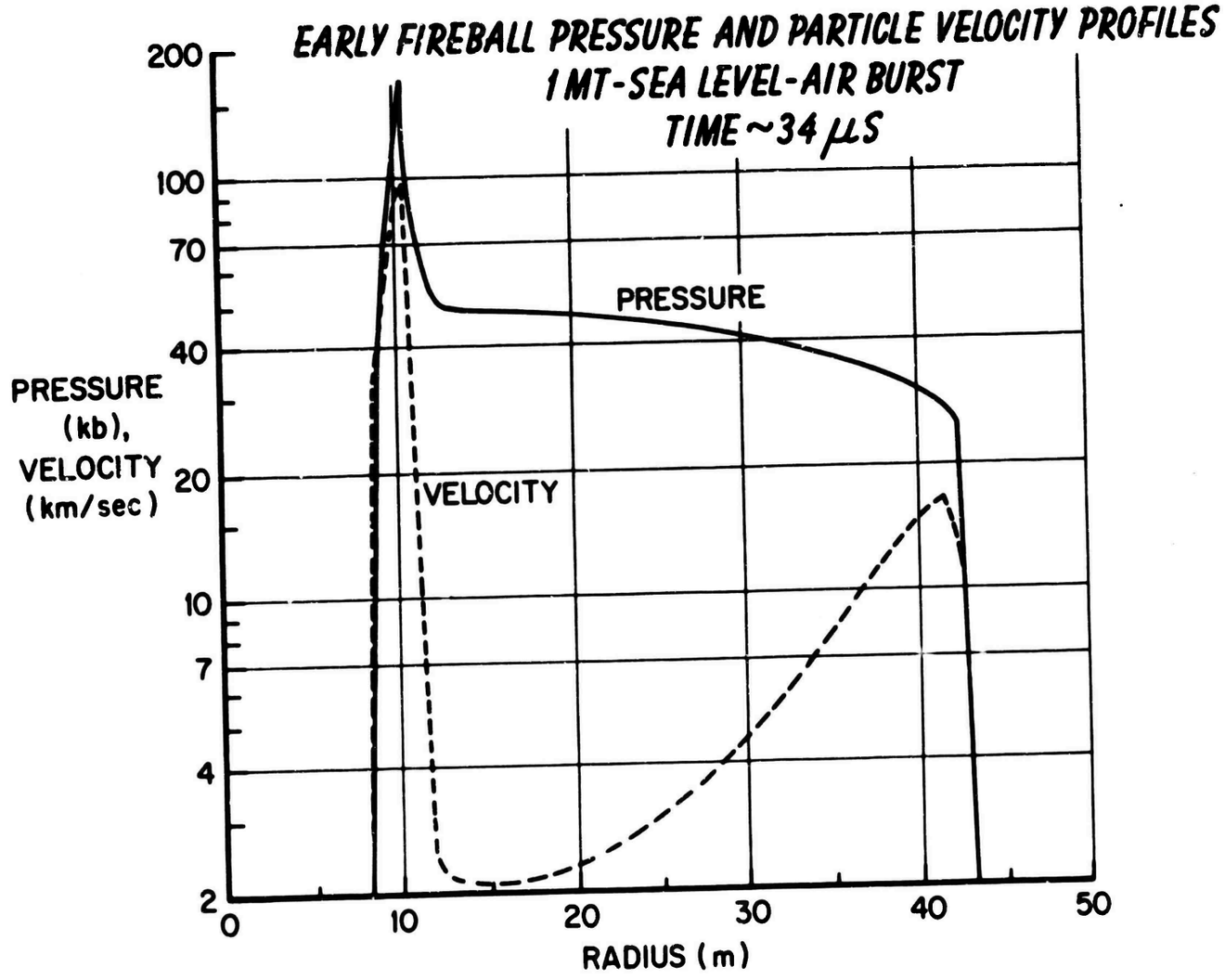
EARLY FIREBALL PRESSURE AND PARTICLE VELOCITY PROFILES
1 MT-SEA LEVEL-AIR BURST
TIME ~ 34 μS
PRESSURE
VELOCITY
PRESSURE (kb), VELOCITY (km/sec)
200
100
70
40
20
10
7
4
2
0
10
20
30
40
50
RADIUS (m)

Fig. 2

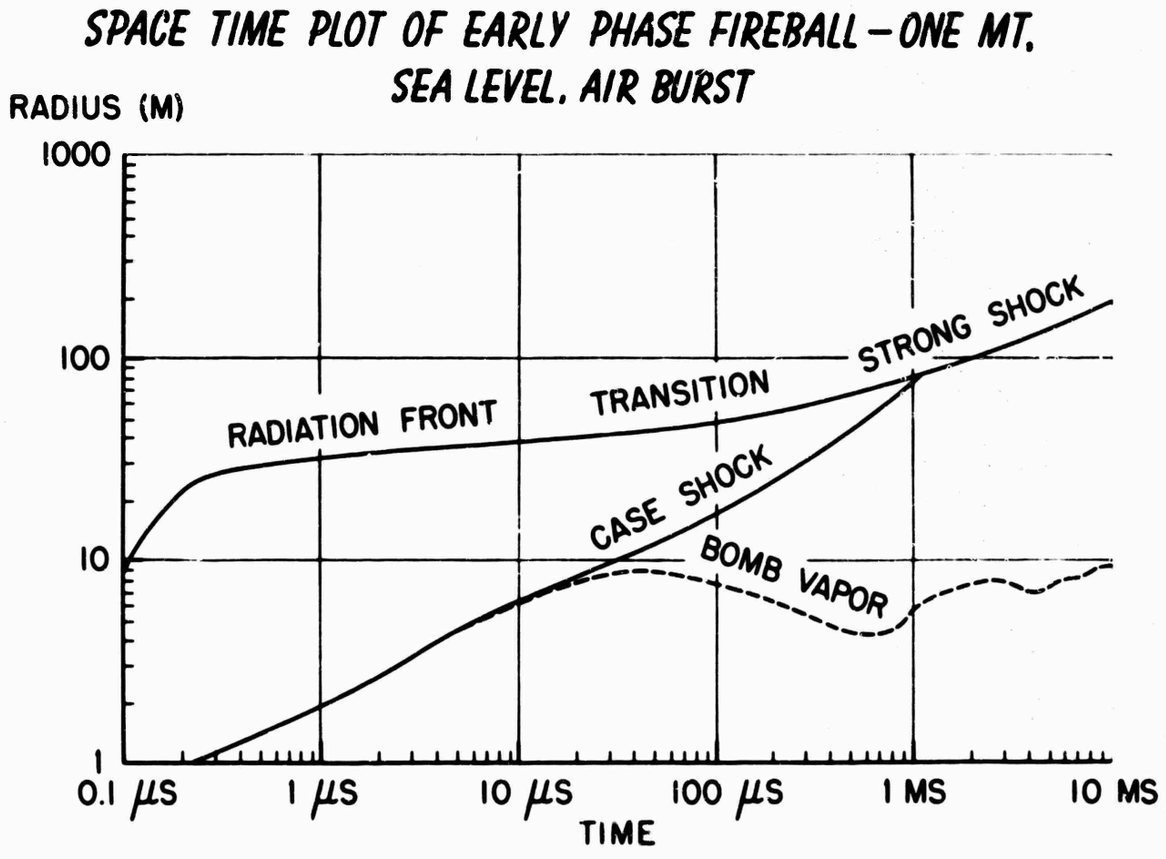
SPACE TIME PLOT OF EARLY PHASE FIREBALL – ONE MT.
SEA LEVEL. AIR BURST
RADIUS (M)
1000
100
10
1
RADIATION FRONT
TRANSITION
STRONG SHOCK
CASE SHOCK
BOMB VAPOR
0.1 μS
1 μS
10 μS
100 μS
1 MS
10 MS
TIME

Fig. 3

Figure 4 shows subsequent temperature profiles as the radiation sphere ceases to expand solely by radiation diffusion and begins to "shock up," expanding by doing work, by pushing the shock wave out through the cold air beyond. In this semilogarithmic plot of temperature versus range for various times, one sees first at the earliest time just the radiation diffusion sphere. At subsequent times, this radiation diffusion sphere is shown to be expanded and cooled as it follows the shock wave, and one sees the shock-heated air as a region of steep temperature gradient beyond the hot interior. At these times, the lowest temperature within the fireball is the fireball front, or the shock front itself, and the fireball radius is coincident with the shock front after the first millisecond.

In Fig. 5 the densities are shown in a similar semilogarithmic plot for the same times. Here, at the earliest times, relatively little compression or expansion has taken place. However, at subsequent times the shock expands and compresses more and more air. The hot interior region drops to lower and lower densities - ultimately to densities (for such a megaton sea level burst) of about 1% of the normal atmospheric density.

Figure 6 is an illustration of this fireball growth transition from a radiation wave to a shock wave. It shows as a function of radius the increase of density at the front, which ultimately becomes the shock front, and it also shows the consequent drop in temperature at this front. As Fig. 6 indicates, the growth of the shock from this radiation sphere does not occur at a single radius but is a gradual process developing over some fair fraction of the initial radius. It should be noted that even after a shock wave is formed the temperatures at the front are still quite high, being measured in hundreds of thousands of degrees kelvin or tens of electron volts. In this figure (Fig. 6) we have temporarily abandoned the one megaton example, since this plot (in both radius and time) is for a one kiloton example. A similar kind of transition occurs in the megaton range, as we shall see shortly.

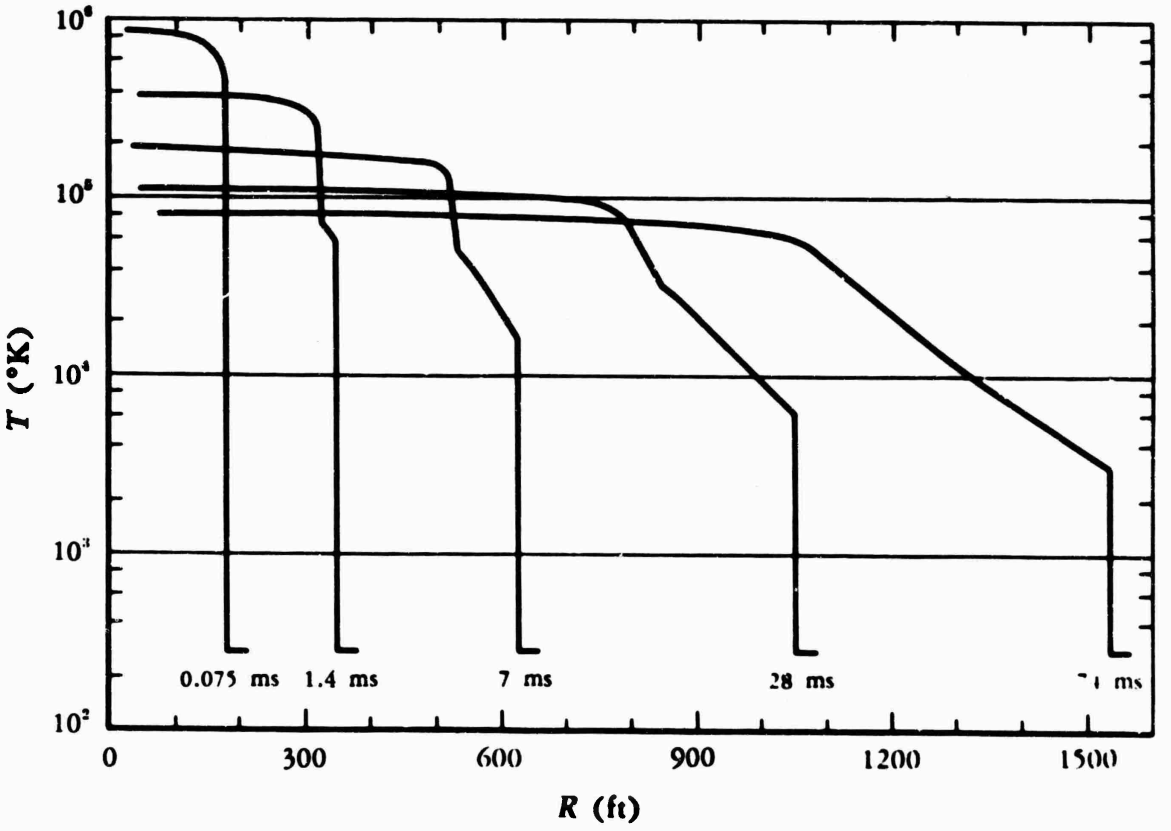

Fig.4—Fireball temperature versus radius at early times in the fireball history (1-MT surface burst)

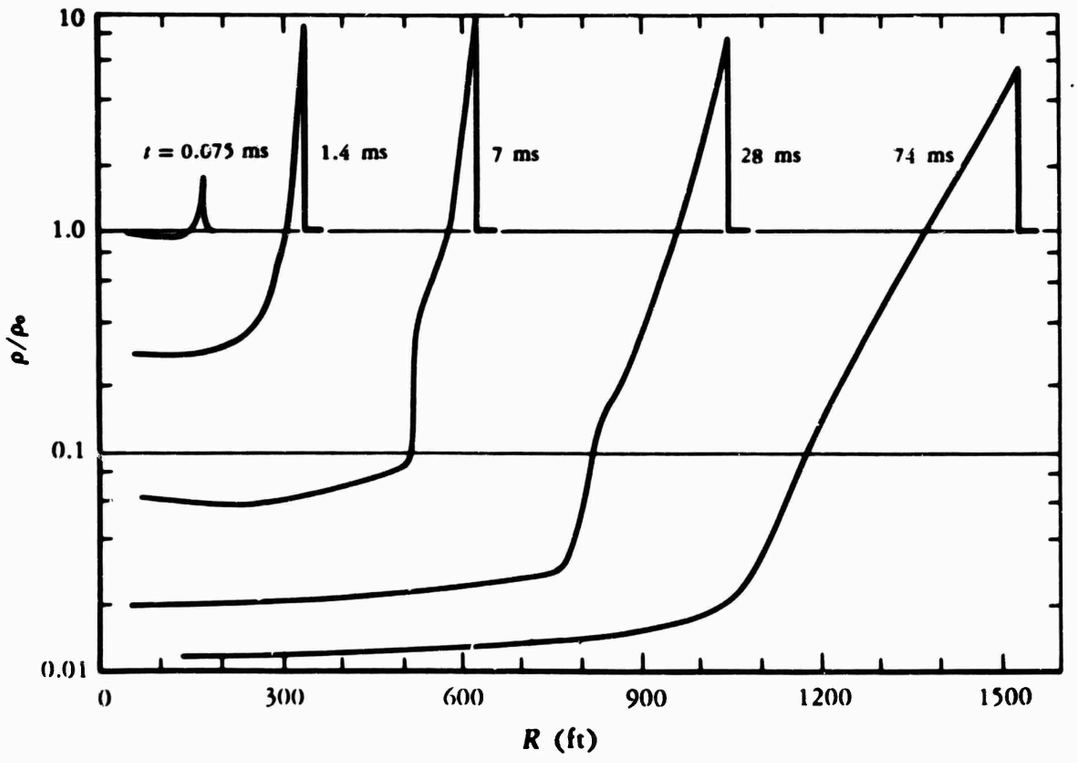

Fig. 5—Fireball density versus radius at early times in the fireball history (1-MT surface burst)

RADIATION DIFFUSION—SHOCK WAVE TRANSITION ONE KILOTON

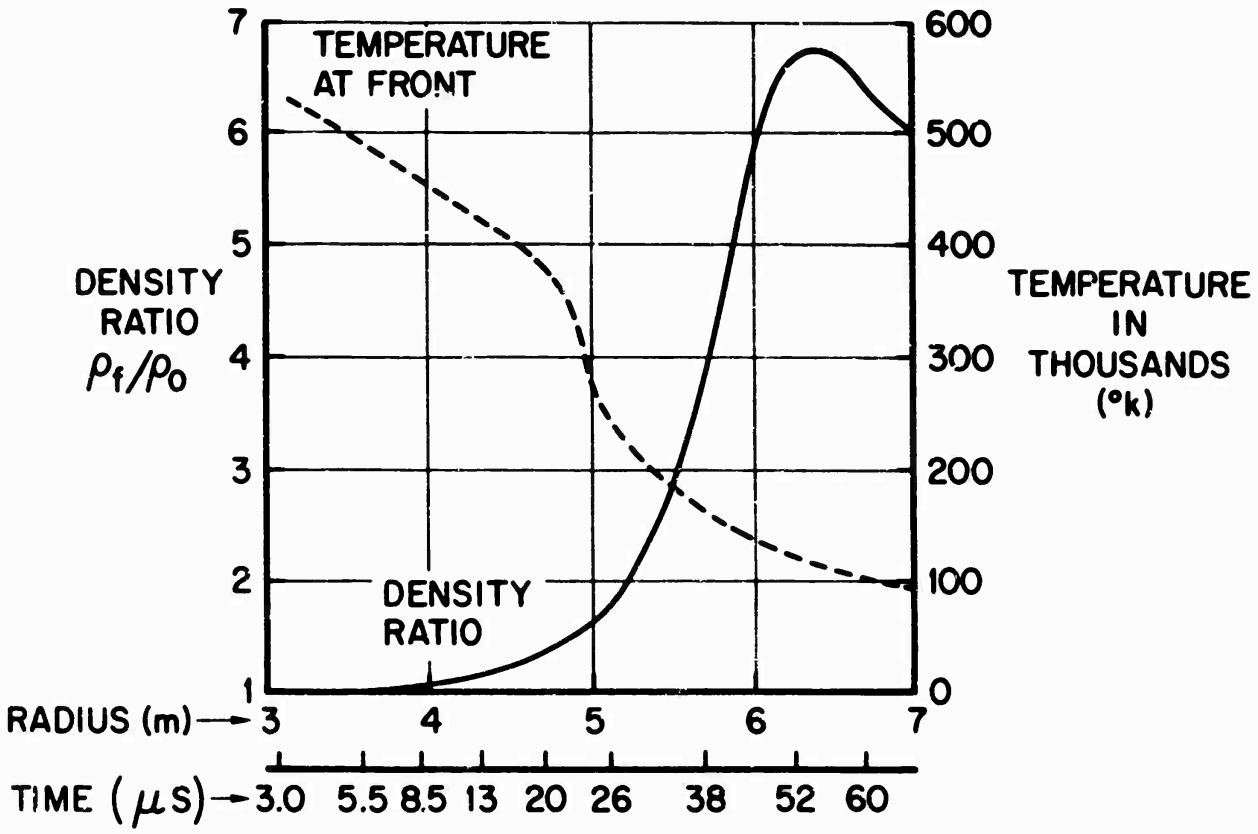

Fig. 6

Figure 7 illustrates the overpressures which occur for the same times as illustrated earlier in Figs. 4 and 5 for the early temperature and density profiles from a megaton explosion. Here, again, one sees the case shock following the radiation front, the radiation front shocking up, the case shock catching up, and forming after a few milliseconds a rather classical strong shock-wave pressure profile. This simple form of the later pressure profiles of Fig. 7 will persist to quite late times, even after the shock wave has become separated from the fireball.

Figure 8 is intended to illustrate the general features of photographs of the fireball during this period after the shock wave has formed, in the time period between the first maximum and the minimum in the light intensity. The most striking feature perhaps of such photographs is the lack of complete symmetry or sphericity. There are frequently relatively large blisters and bright spots associated with this glassy looking shock front. These are evidences of the non-ideal nature of fireballs, or rather of features of nuclear explosions, which are not adequately covered in current theoretical models of fireball growth. Quite likely, these are blobs of bomb vapors which are thrown at high velocities against the back of the shock wave. They were accelerated in the earliest phases of the weapon's expansion and remained in dense clumps or jets while the fireball was expanding and so were not subject to as much drag deceleration. Since the fireball expansion slows rapidly after its initial radiative growth, such blobs ultimately overtake the fireball front, splashing against the high density of the back of the shock. The steep gradients in temperature within the fireball are also illustrated in this figure, showing that although the shock front is the lowest temperature one sees, the interior can still be at extremely high temperatures and yet continue to be obscured by the outer shock-heated air.

Figure 9 illustrates one of the difficulties in scaling some fireball features. It offers a comparison of curves of shock density (relative to ambient density) during the transition from a radiation sphere to a shock fireball between a number of examples of different yields and (in each case) different nuclear explosion source models.

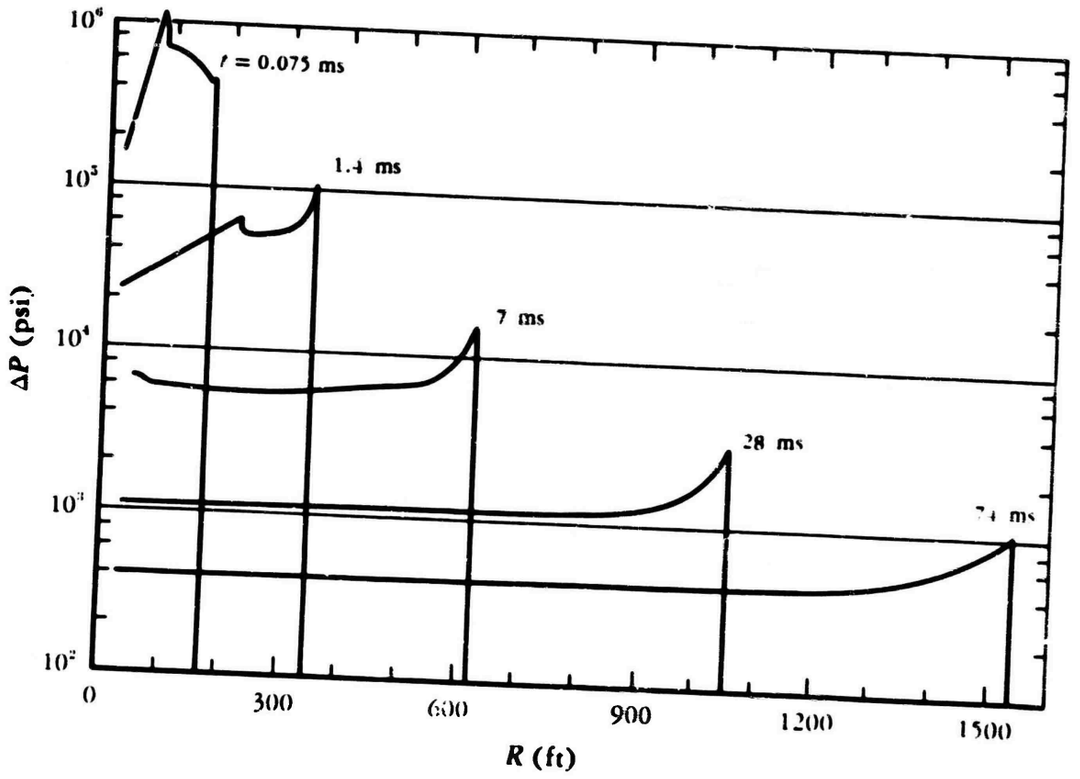

Fig. 7—Overpressure versus range at early times in the shock-wave growth (1-MT surface burst)

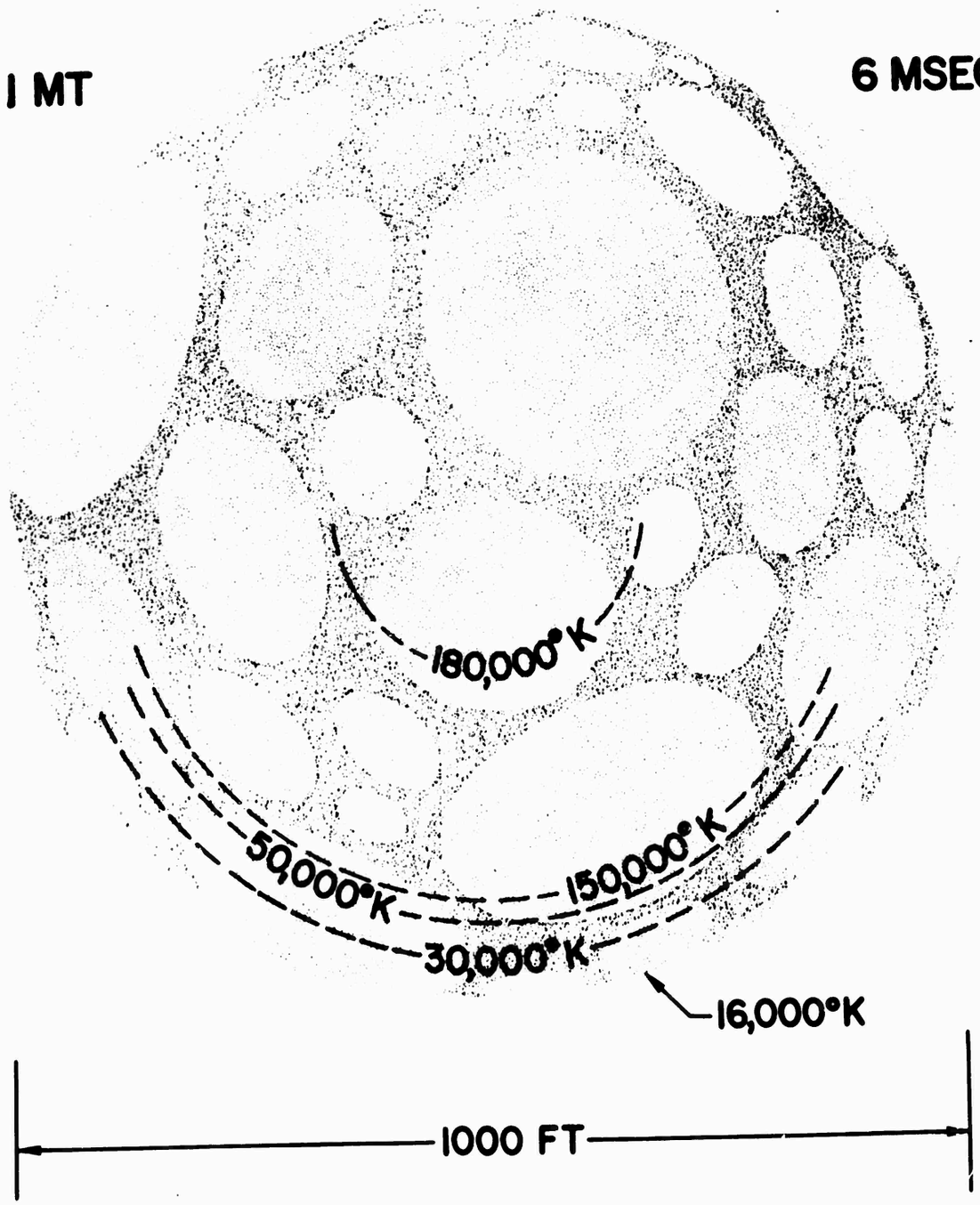

Fig. 8—Early fireball size and temperature
(while shock front is opaque)

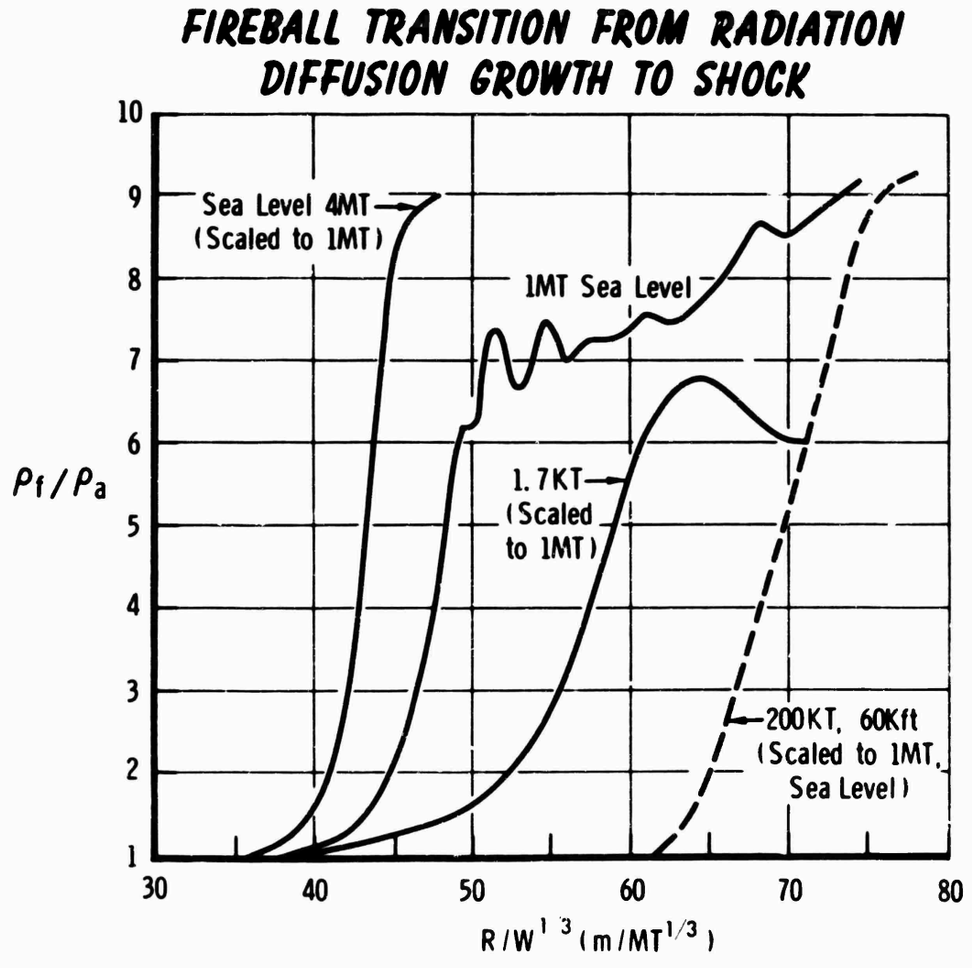
FIREBALL TRANSITION FROM RADIATION DIFFUSION GROWTH TO SHOCK
Sea Level 4MT (Scaled to 1MT)
1MT Sea Level
1.7KT (Scaled to 1MT)
200KT, 60Kft (Scaled to 1MT, Sea Level)
ρ_f / ρ_a
$R/W^{1/3}$ (m/MT$^{1/3}$)
10
9
8
7
6
5
4
3
2
1
30
40
50
60
70
80

Fig. 9

In particular a rather heavy four megaton bomb was used, while a lighter one megaton version was included along with a still different one kiloton bomb. In Fig. 9, all are scaled to one megaton by the cube root of the yield. This comparison shows that this scaling is not an appropriate scaling to apply to this transition radius or time. Also indicated is a 200 kiloton example for a different altitude, scaled to the one megaton radius by the cube root of the yield again, and also scaled by the cube root of the ambient density ratio between the 60,000 foot altitude ambient density and that at sea level.

From this figure, Fig. 9, it is clear that something other than the simple cube root or volumetric scaling with yield is necessary to properly scale the shock transition radius. The altitude scaling as with the cube root of the ambient density also fails to be useful, as we shall see more clearly later.

A similar comparison of the fireball front temperatures as a function of time for these three calculational examples is illustrated in Fig. 10. Note that the sudden drop as the shock forms also fails to scale by the cube root of the yield. However, the late time temperatures of the front, which by then is the shock front, are relatively well represented by the cube-root scaling.

Figure 11 shows for the same three examples the interior temperatures as a function of time scaled in the same way. This figure indicates an even more serious failure of scaling, in the direction which one might expect, however. A small yield fireball has at scaled times relatively fewer mean free paths for radiation than a large yield fireball, and so would tend to radiate at a relatively faster rate and to cool more quickly. These temperatures are shown at times when the radiation diffusion can still be influential in reshaping the fireball interior.

Much of the indicated difference between the four megaton and one megaton case in this figure is due to a difference in weapon models and in the fraction of the yield emitted in the early x-ray emissions, a larger fraction being allowed in the megaton example.

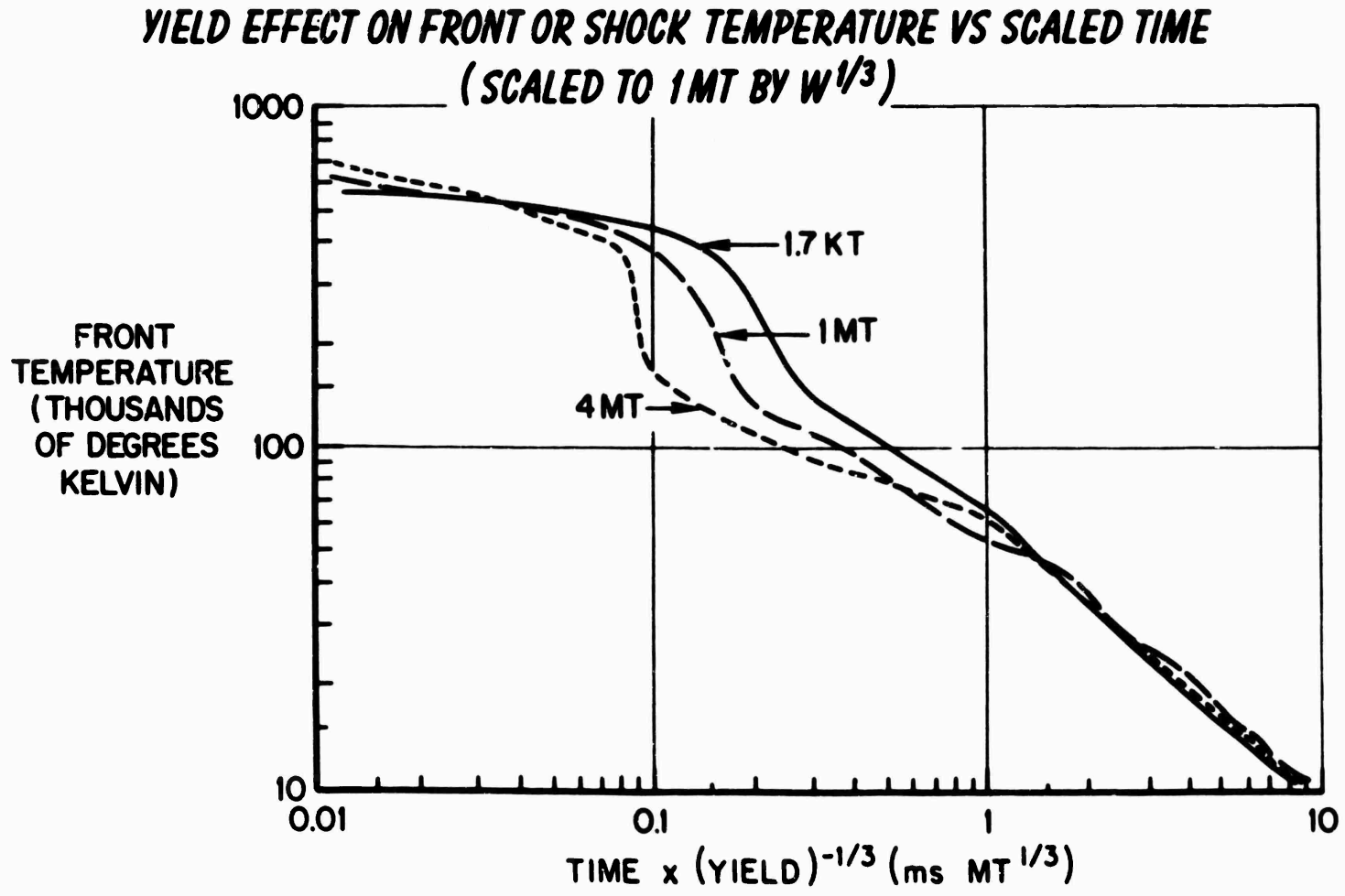
YIELD EFFECT ON FRONT OR SHOCK TEMPERATURE VS SCALED TIME
(SCALED TO 1 MT BY W^1/3)
1000
100
10
FRONT TEMPERATURE (THOUSANDS OF DEGREES KELVIN)
1.7 KT
1 MT
4 MT
0.01
0.1
1
10
TIME x (YIELD)^-1/3 (ms MT^1/3)

Fig. 10

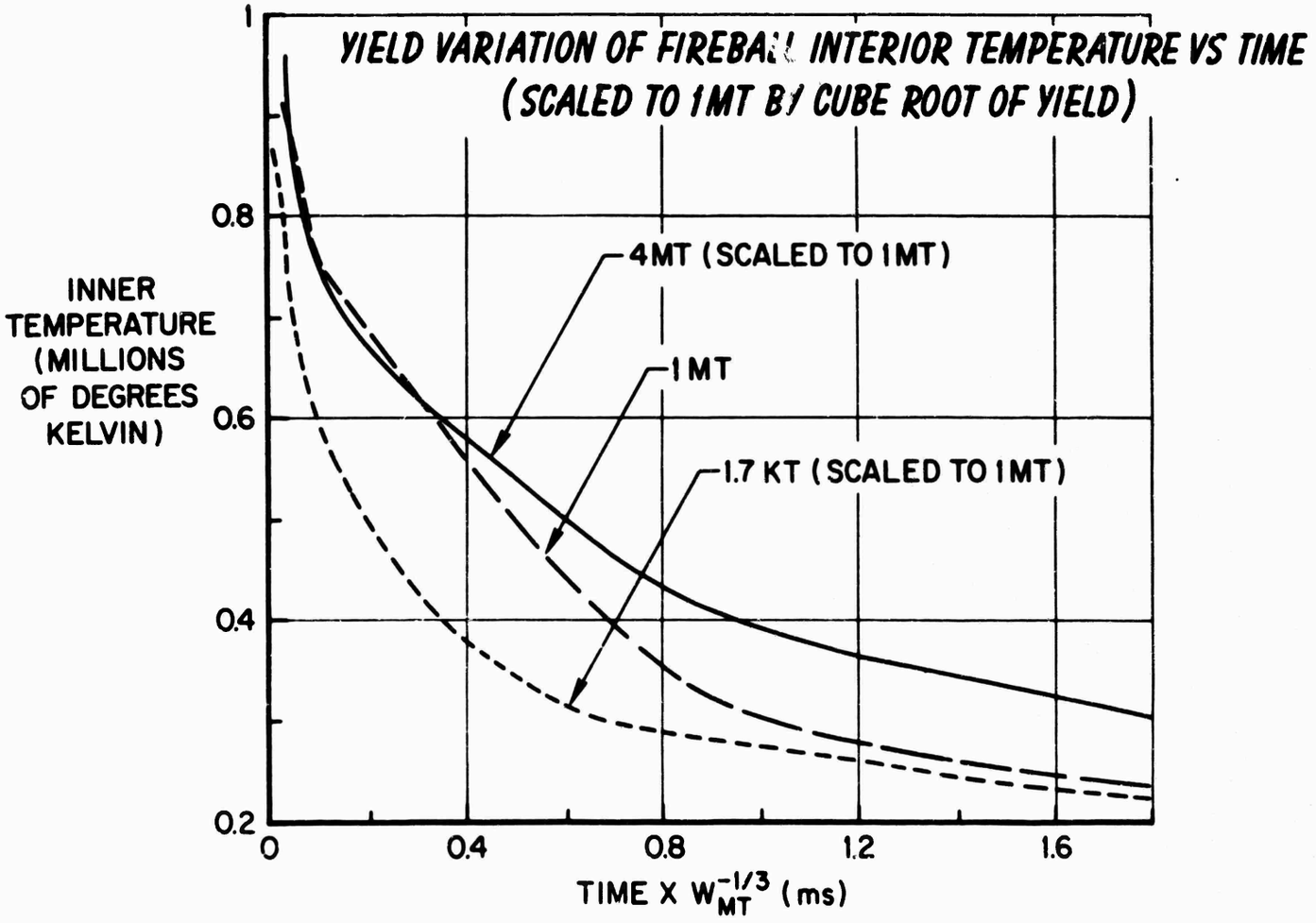
YIELD VARIATION OF FIREBALL INTERIOR TEMPERATURE VS TIME
(SCALED TO 1MT BY CUBE ROOT OF YIELD)
INNER TEMPERATURE (MILLIONS OF DEGREES KELVIN)
1
0.8
0.6
0.4
0.2
4MT (SCALED TO 1MT)
1MT
1.7 KT (SCALED TO 1MT)
0
0.4
0.8
1.2
1.6
TIME X $W_{MT}^{-1/3}$ (ms)

Fig. 11

Figure 12 illustrates a number of these features for the three calculational examples in the radius-time context, all scaled, of course, to one megaton by the cube root of the yield. Here, the radius of the radiation diffusion front fails to scale to the extent that the fraction of the energy radiated is different in the different examples. The radiation front for the one megaton example scales to a relatively larger radius because the bomb model used was a hotter bomb, and a larger fraction of its one megaton yield was radiated in the early x-ray yield. In the four megaton example, a somewhat smaller fraction was allowed out in this x-ray pulse. For the 1.7 kiloton example, of course, a much smaller fraction was emitted and it was at a much lower rate. But, conversely, the fraction of the energy remaining in the case shock is relatively larger in the kiloton example than in the megaton examples so that the case shock scaling is likewise not appropriately represented by a simple cube root of the total yield scaling. The one feature which is clearly <u>well</u> represented by such a scaling is the main shock <u>after</u> the shock transition and <u>after</u> the joining of the case shock with the fireball shock. The debris motion, of course, will be quite different for different yields and will not be scalable in the same way, since the motions of the debris are more dependent on the momentum or inertia in the bomb vapors, and, therefore, on the mass more than on the energy of the debris. Consequently, on a yield scaled basis, a kiloton example shows larger expansion of the debris than in a megaton example. In any case, these theoretical hydrodynamic models can not adequately account for the expansion of the debris, which, at an early stage, becomes turbulent, establishes jets, and results in motions which are not included in the symmetric hydrodynamic calculation.

One could study each feature of these early phases and derive more appropriate scaling criteria. For an example, as illustrated in Fig. 13, one might select a different fractional power of the yield by which to scale the radius or time at which the transition from radiative growth to shock growth occurs. A power somewhat between the cube root and the fourth root appears best for the scaling with yield of the transition radius. Figure 13 suffers

YIELD SCALING OF EARLY SPACE-TIME FEATURES

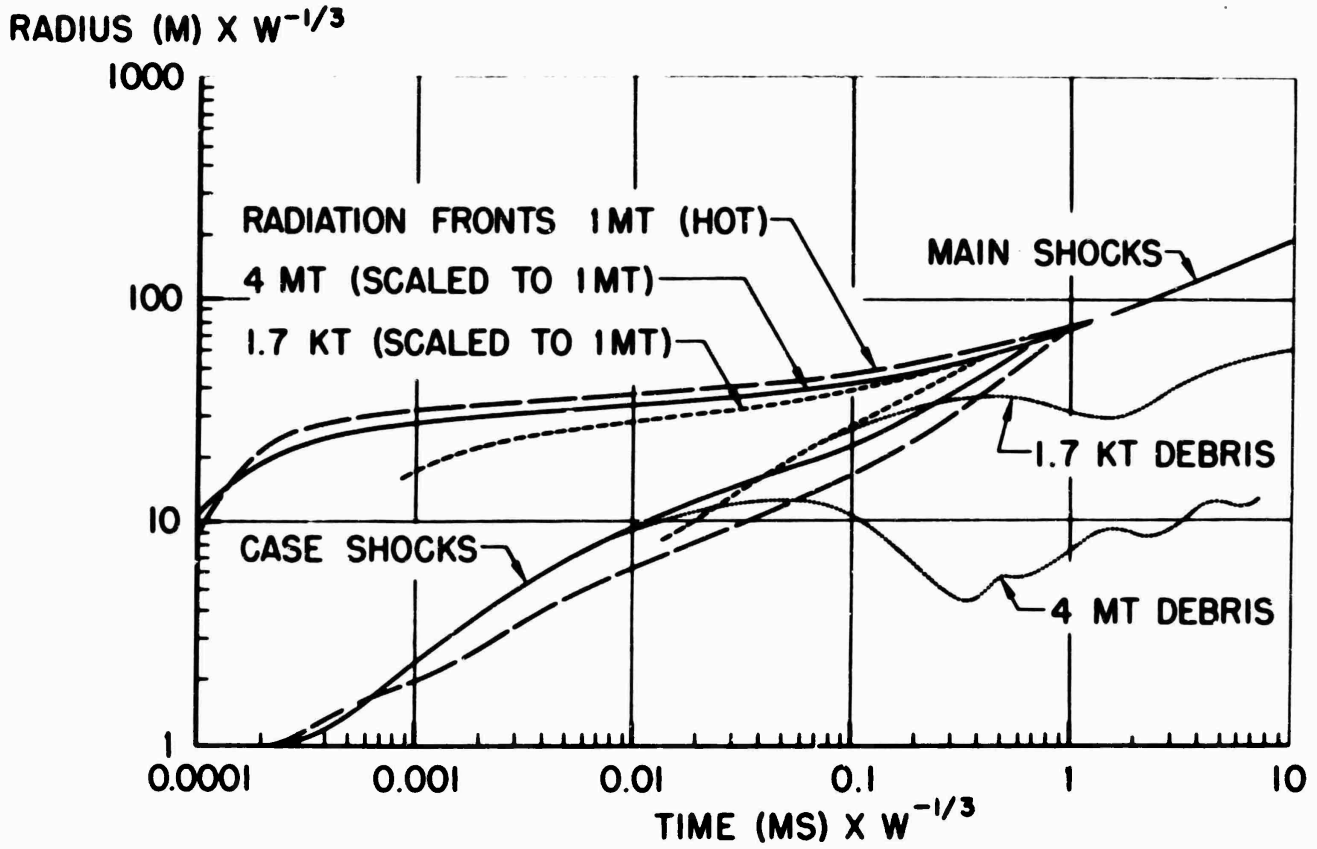

Fig. 12

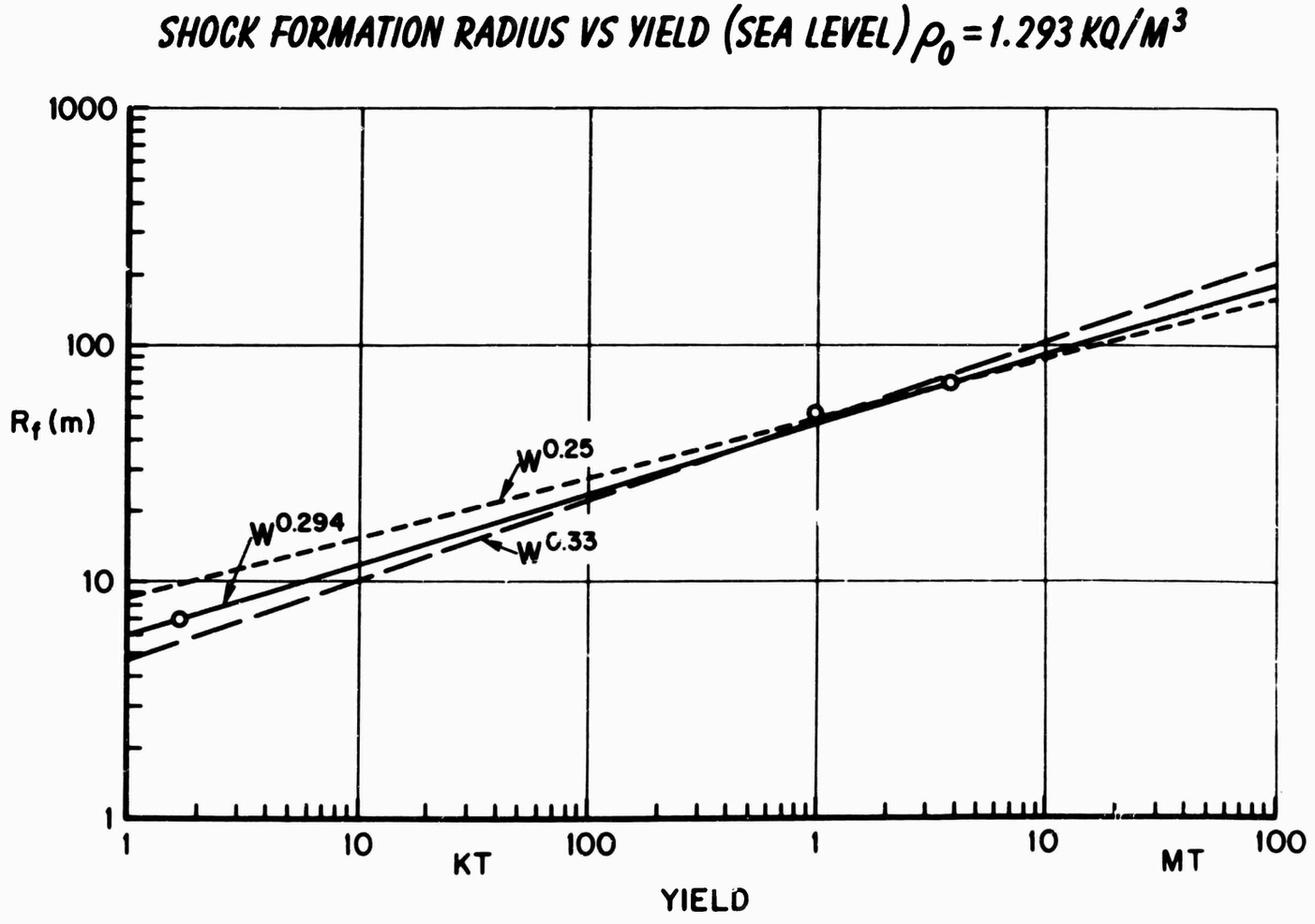
SHOCK FORMATION RADIUS VS YIELD (SEA LEVEL) $\rho_0 = 1.293$ KG/M^3
1000
100
10
1
R_f (m)
$W^{0.25}$
$W^{0.294}$
$W^{0.33}$
1
10
KT
100
1
10
MT
100
YIELD

Fig. 13

from paucity of calculational cases on which to base a scaling, but does show a clear trend different from either cube root or fourth root over at least three orders of magnitude in range of yields. A more definitive basis for scaling would certainly result from a compilation of more calculational examples, although such further results might indicate that no simple power-law scaling would be appropriate, i.e., that the scaling does not follow a constant slope on such a log-log plot, but may in fact lead to different slopes in different regimes or ranges of yield. What is also clear is that scaling of such phenomena as this radius for transition would be more sensibly based on the radiative or x-ray yield fraction rather than on the total yield, since this fraction can change both as a function of the yield and as a function of the bomb design.

Figure 14 is intended to illustrate the lack of significant features in the photographs of fireballs at a stage near the minimum in light intensity. At a time of about 80 milliseconds for this example of one megaton at sea level, the shock wave has expanded and weakened to such an extent that the shock temperature is relatively low, of the order of 2000^{o}, at which temperature air is no longer strongly luminous. For this reason, we begin to see through the shock front into the hotter interior. Subsequently, as the fireball continues to expand and the density continues to drop in the interior, the temperature to which we can see rises and the intensity of thermal radiation rises appropriately. Although the shock wave continues to expand, eventually the hot interior region which is the late fireball slows and finally ceases to grow. The shock wave by then has become separated and quite independent of this late fireball.

Figure 15 illustrates the temperature profiles that would be typical of a one megaton sea level explosion in this late time period. As the thermal radiation depletes the energies of the fireball interior at the times approaching a second, the temperatures in the interior drop markedly to temperatures of the order of five or six thousand degrees, below which the radiation rate is extremely slow.

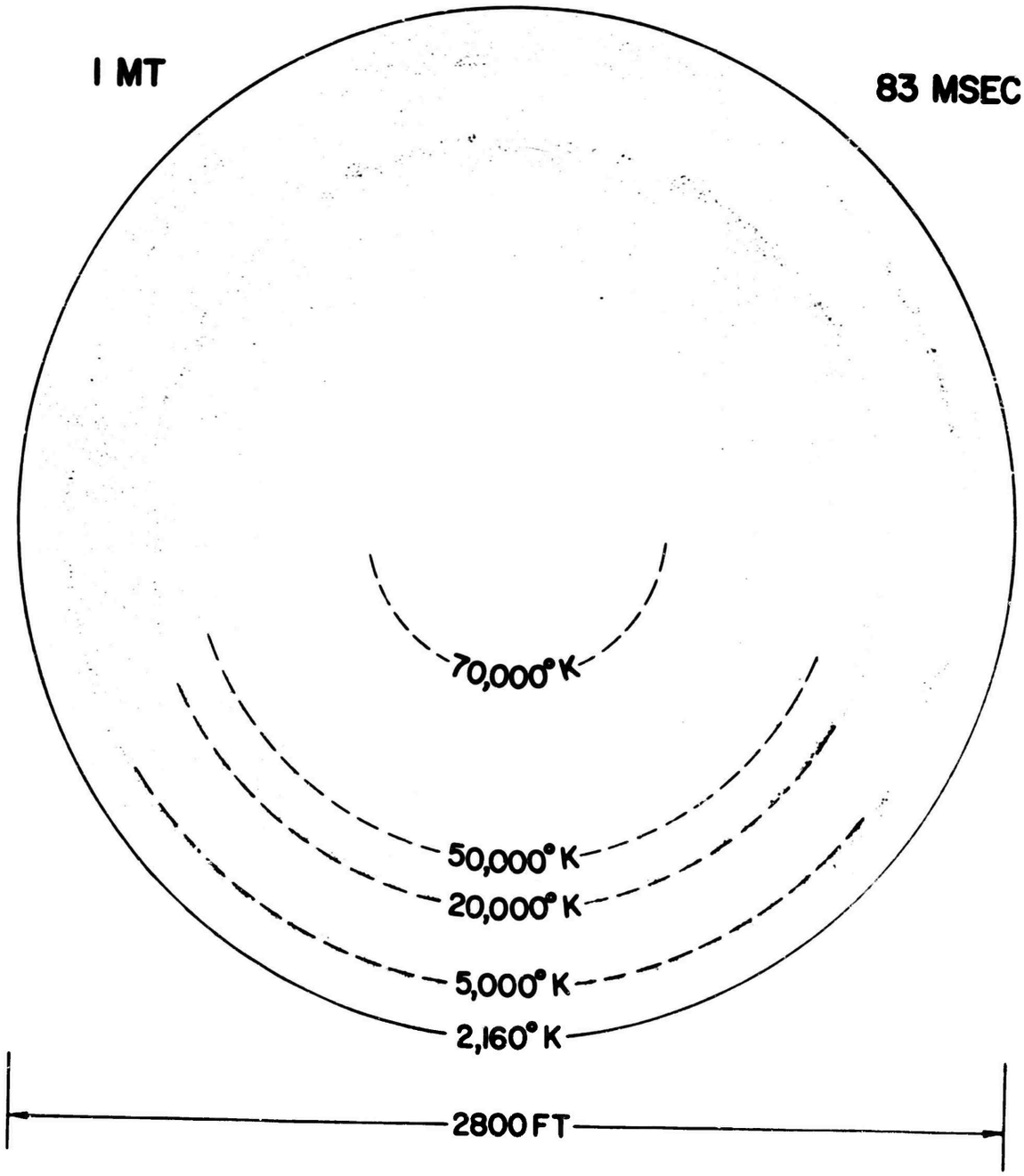

Fig. 14—Fireball size and temperature at a time near minimum light intensity

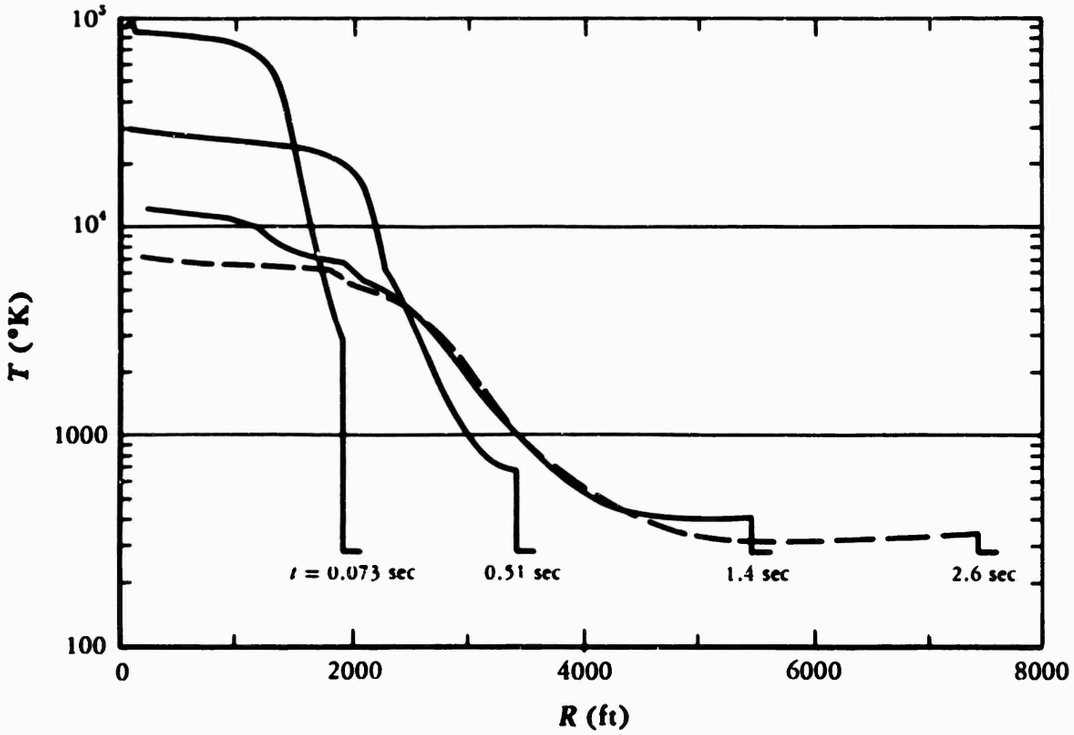

Fig. 15—Late fireball temperature versus radius

The corresponding late-time densities are illustrated in Fig. 16. The gradual slowing down and depletion or the dissipation of the fireball itself is again evident in the extent of low density air. At times of several seconds a low density sphere (of modestly high temperatures) is left, which then further cools mostly by rising and mixing in the atmosphere. Of course, at these late times, beyond the time of the maximum intensity in thermal radiation, one can expect to see completely through the system of shock waves and fireball air and to see, then, the bomb vapors themselves.

Figure 17 indicates something of this late time fireball temperature structure for this one megaton example at 1.3 seconds.

Figure 18 illustrates the temperature history within and close to the fireball. The different curves are characterized by the peak overpressure of the shock at those distances for this one megaton example. For instance, the 100 psi point is at a distance from the point of burst of approximately 850 meters. Whereas this 100 psi point is about at the edge of the fireball, the 40 psi distance (1500 m) is clearly outside the fireball, and it experiences a far less severe temperature history. The 200 psi point, at a distance of about 640 meters, experiences temperatures in the thousands of degrees for a matter of several seconds. For such a fixed point on the ground or above it, the temperature ultimately drops back to normal as the fireball rises away from it in the atmosphere. Most of the rise occurs after the shock wave and the thermal radiation have played out their roles in the fireball development. The dashed curve which drops from the 200 psi curve indicates the nature of this temperature drop due to such fireball rise. The other curves show a continued high temperature, but do not at these late times represent a realistic model in that the calculation which provided these numbers did not include any of the gravitational mixing and rising effects which continue to cool the fireball interior.

Although these temperatures at very close-in distances are indeed impressive, the response of materials for such a relatively short exposure is by no means simple, and can by the use of straightforward thermal diffusion predictions be much exaggerated. The dynamics of

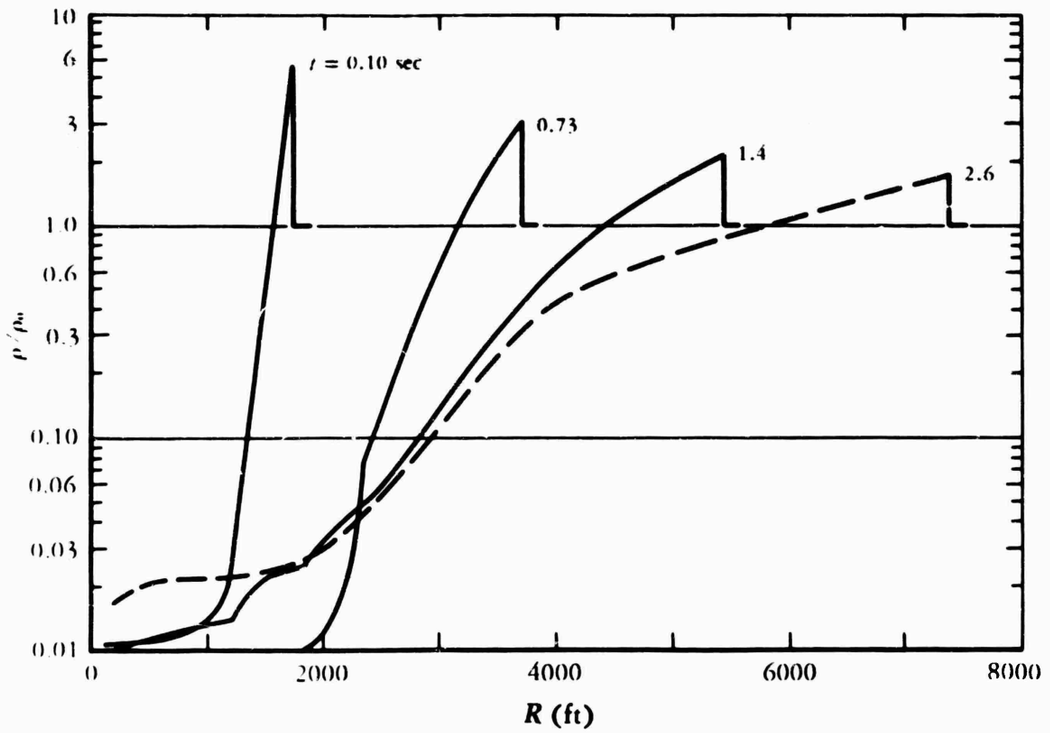

Fig. 16—Late fireball densities (1-MT surface burst)

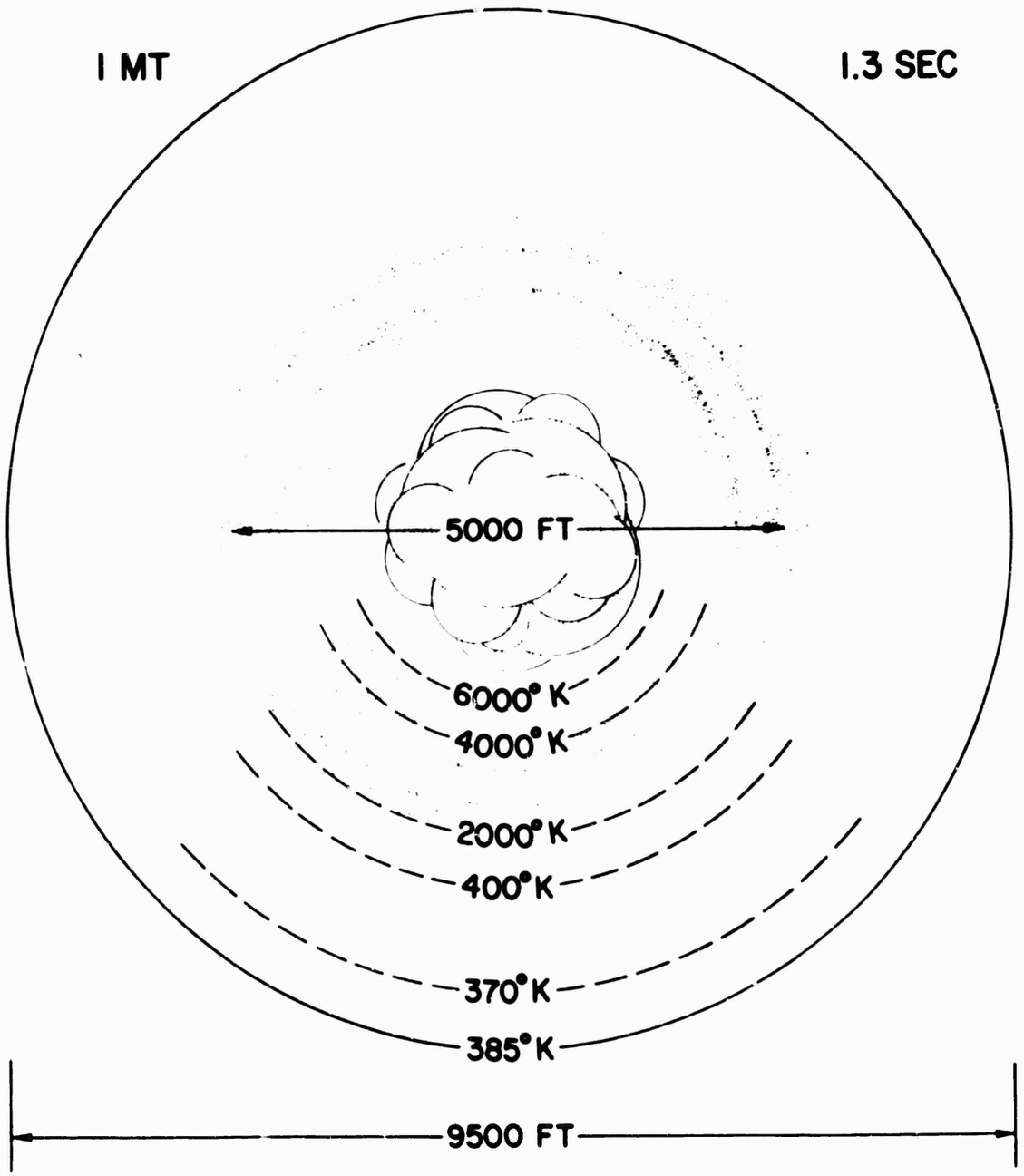

Fig. 17—Late shock and fireball size and temperature

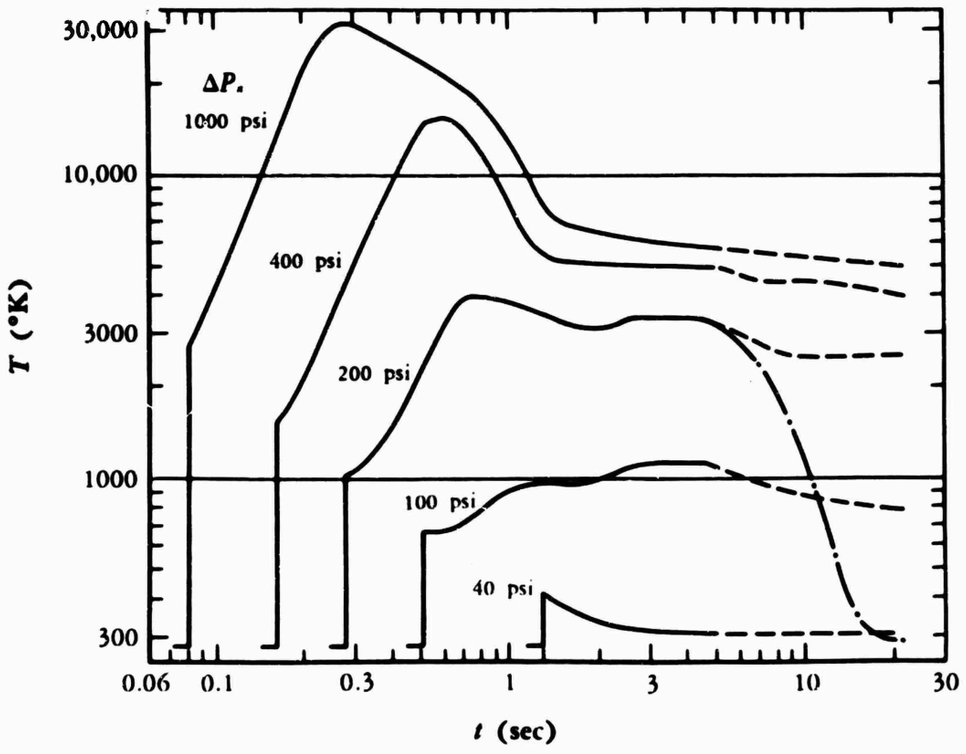

Fig. 18—Temperature versus time at high peak overpressures (1-MT surface burst)

the surface interactions is such as to provide considerable protection against ablation for relatively long times.

Figure 19 illustrates an interesting feature in the fireball growth, which is: the continued effect of radiation diffusion even after a shock wave is formed at the fireball front. Here is a Lagrangian plot (a plot which follows the history of certain air particles) versus time for air particles which were shocked to temperatures of 40,000 to 20,000 and to 10,000 degrees. After the shock arrival (which is the sharp rise) the air particles begin to cool in the expansion behind the shock, but at a later time these particular air masses are overtaken by the advancing radiation diffusion front and are then reheated even while continuing to expand behind the shock wave. This effect is seen to decrease rapidly, so that out in that air which is struck by a $10,000^{\circ}$ shock, there is relatively little subsequent heating due to any continued radiation diffusion.

Most of these considerations so far have been in the absence of a number of features which are frequently important if not dominant in determining the character and the phenomena of the fireball. Figure 20 is meant to illustrate some of these imperfections or some of these complicating features when an explosion takes place close to other materials, as in a surface burst. It is possible that large quantities, indeed, for a surface burst - literally megatons of earth material (for megatons of explosion yield) - become involved in the fireball gases at a very early stage. That is, much of the cratered material is thrown up into (and intimately mixed with) the fireball at a time prior to its thermal radiation maximum. Such large amounts of material must have a considerable influence on the nature and the timing of the subsequent thermal radiation and, indeed, on the total amount of radiation. It does, of course, have a marked effect on the fireball, as evidenced by high speed pictures. The fireballs are by no means spheres nor are they rigorously even segments of spheres; there are frequently perturbations of precursor-type shock waves on or near the surface which further obscure a portion of the fireball. There are numerous

TEMPERATURE HISTORIES OF AIR PARTICLES SHOCKED TO 40,000, 20,000 AND 10,000 °K, SHOWING EFFECT OF CONTINUED RADIATION DIFFUSION AFTER SHOCK FORMATION

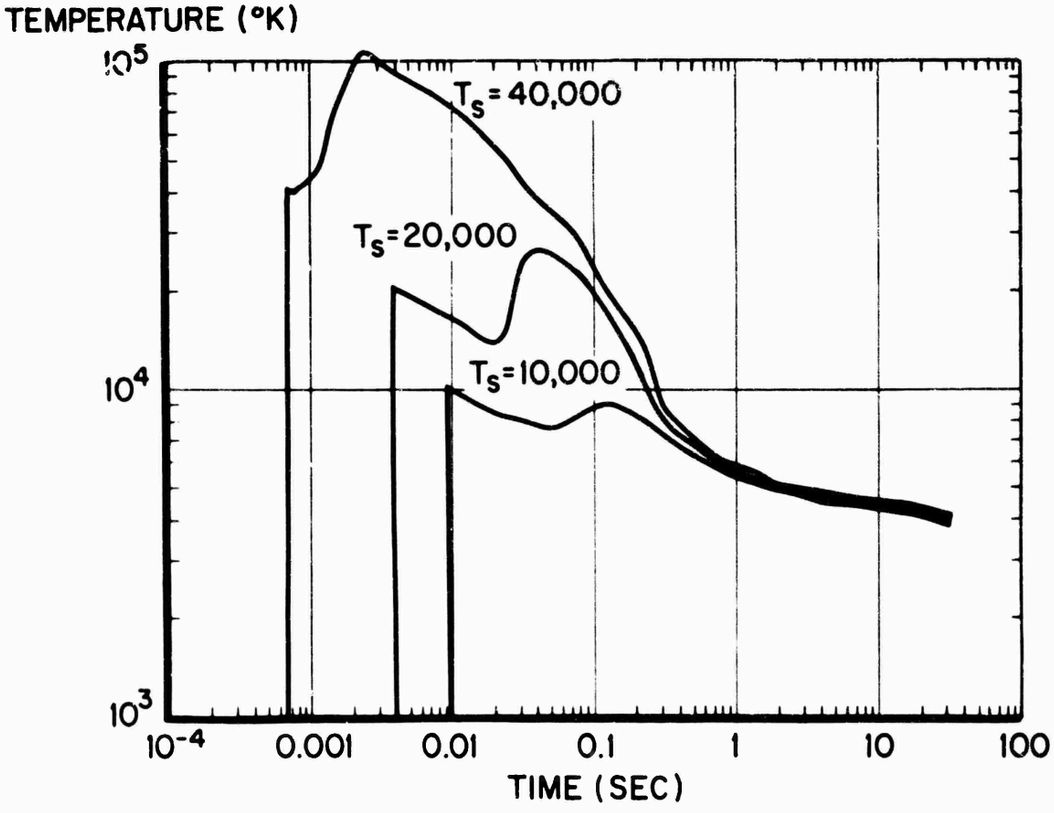

Fig. 19

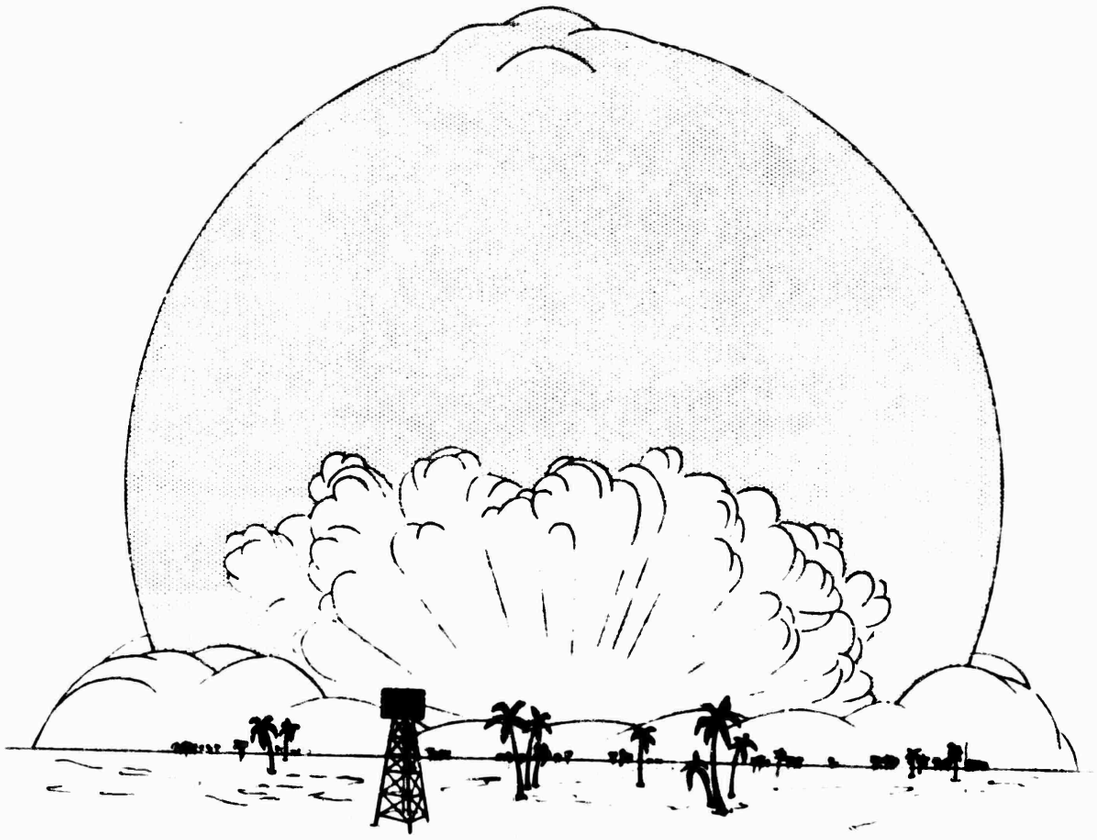

Fig. 20—Surface burst features influencing thermal radiation

reflected shocks being transmitted back through the fireball which further change its state (Fig. 21). In the latest time periods the vast amounts of debris so entrain the energy, and provide such an increase in the opacities, that the rate of radiation may be more determined by the rates at which the hot gases are brought to the surfaces of turbulent vortices rather than by any radiation transport rates. The complicated state of affairs in the late stages are meant to be suggested by Fig. 22 for such surface and near surface bursts.

In general, then the prediction of various fireball phenomena as a function of yield for surface bursts should properly include a number of other conditions, such as some detail of the weapon and/or any other materials at or near the point of burst. Such additional information is necessary in order to predict with accuracy each of the fireball features which we have been discussing. When we consider the effect of the atmosphere on fireball phenomena and become concerned with scaling of these phenomena to other altitudes of burst above sea level, we are faced with such further complications as the equation of state of air whose specific heat increases somewhat as one goes to higher altitude. Perhaps of more importance are the optical properties of the air which change more markedly with varying ambient density, leading to longer mean free paths or lower absorption coefficients at high altitudes.

Figure 23, for instance, illustrates something of the change in the equation of state. It shows the ratio of pressure to energy per unit volume as a function of the air temperature for various air densities relative to sea level air (from air ten times normal density to one millionth of normal density). The salient feature of this set of curves arises in the fact that at very low densities, and in some temperature ranges, the pressure can be very low while the energy per unit volume remains high. In fact, for low densities this ratio can become less than half of what it is for sea level air at temperatures around $10{,}000^{\circ}$. Such temperatures are critical to the fireball since this is a temperature characteristic of the period in which much of the thermal radiation is emitted.

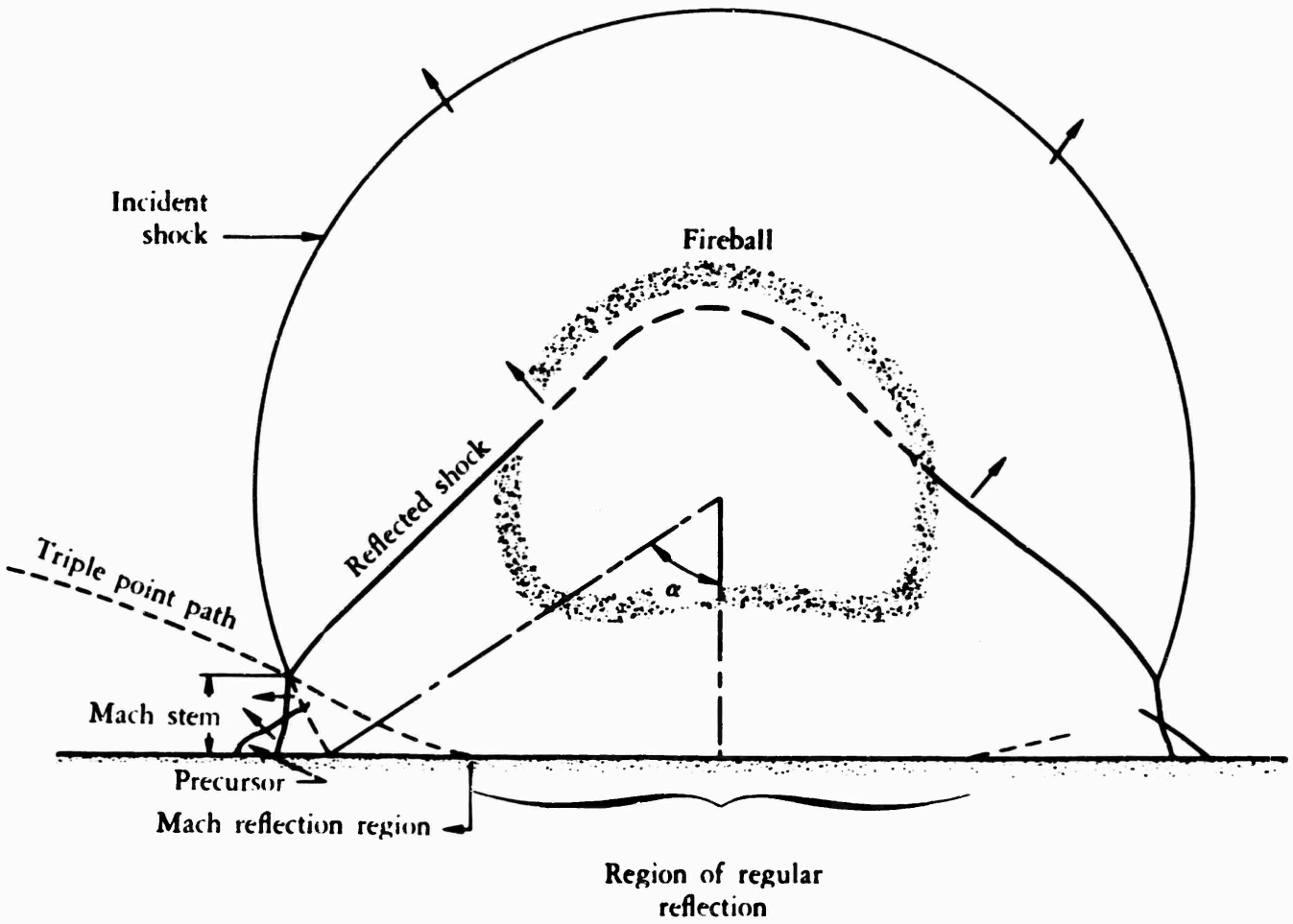

Fig. 21 — Shock configurations (air burst)

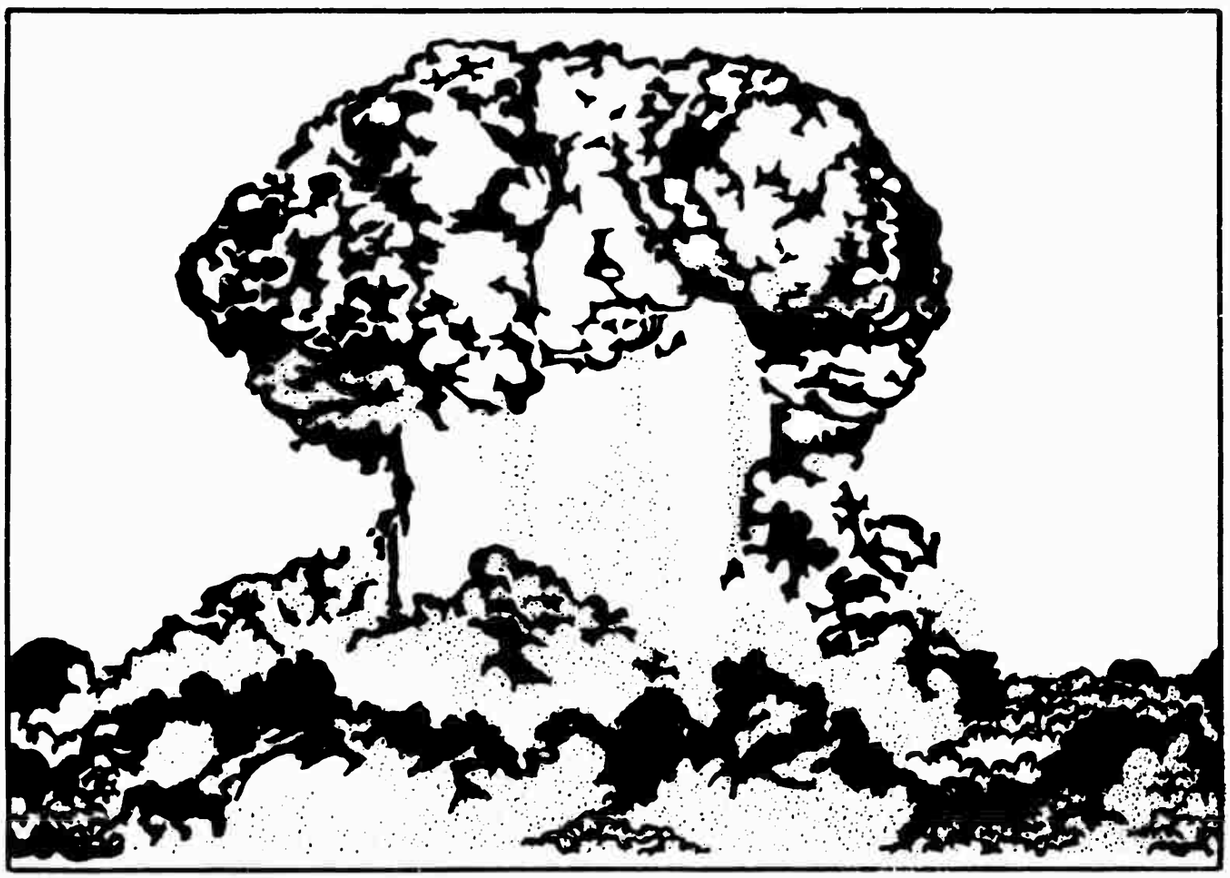

Fig. 22—Turbulent mixing from late fireball or early cloud

PRESSURE-ENERGY PARAMETER, $\gamma - 1 = p/\rho E$, FOR AIR AT VARIOUS DENSITIES, AS A FUNCTION OF TEMPERATURE

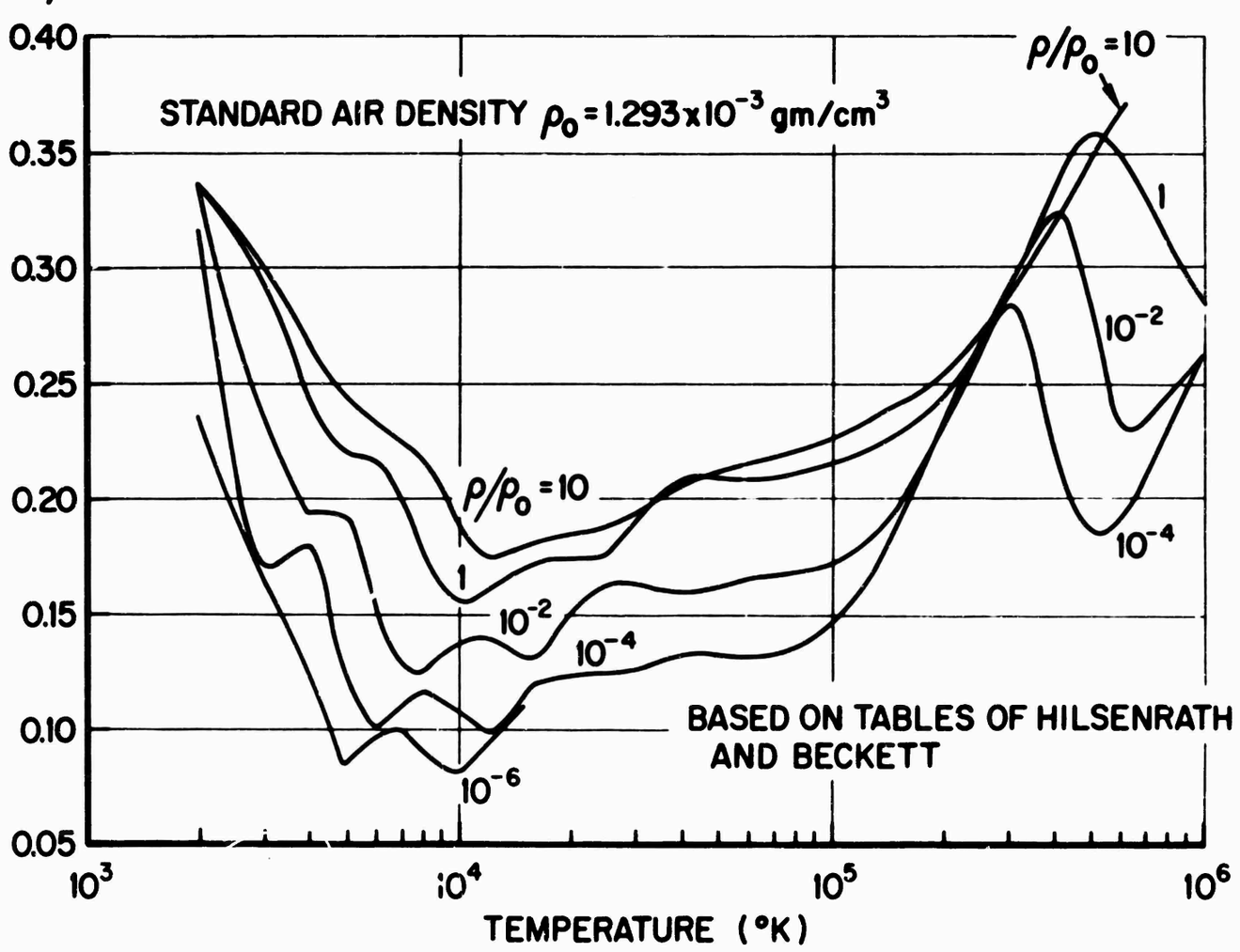

Fig. 23

This disparity in the relation between pressures, temperatures, and energies is likely to result in some differences in the blast wave and, therefore, in the rate of expansion of fireballs; but a more serious change in the properties of fireballs is characterized by the optical property changes with density. One such indication is illustrated in Fig. 24 which shows curves of the Rosseland mean free path for radiation in air as a function of temperature for a similar range of densities. Here, it is evident that over much of the temperature history of the fireball at sea level (where densities at the front or in the shocks are at least normal or greater than normal), much of the mean free paths are less than a meter and often as short as a few centimeters to even fractions of millimeters. In any case, at sea level the mean free paths are much shorter than fireball dimensions at all temperatures. On the other hand, for high altitude explosions, where the densities are small fractions of the sea level density, the mean free paths may become everywhere long and indeed eventually can become much greater than the size of the fireball itself, so that radiation properties must be markedly different in such cases.

For altitudes of burst where mean free paths are not yet long compared to fireball dimensions, the same kind of calculations (using the diffusion approximation) can be carried out. Figure 25 illustrates the density growth (the shock density development) for a number of such high altitude examples, all scaled to 200 kilotons and scaled in radius by the cube root of the ratio of the ambient density to that at sea level.

These examples illustrate again the failure of the simplist scaling for the very reasons which we have hinted at in the lack of scaling of optical properties or of the radiation growth properties. It is seen that the sea level calculation shocks up or ceases to expand radiatively at the earliest time or at the smallest radius, whereas the successively higher altitude cases require a larger radius and lower fireball temperatures before a shock wave becomes the dominant mechanism of expansion. Indeed, at the highest altitudes, the whole model or mechanism of creating the fireball becomes signifi-

ROSSELAND MEAN FREE PATH FOR AIR—USED IN RADIATION DIFFUSION CALCULATIONS ($\eta = \rho/\rho_0$)

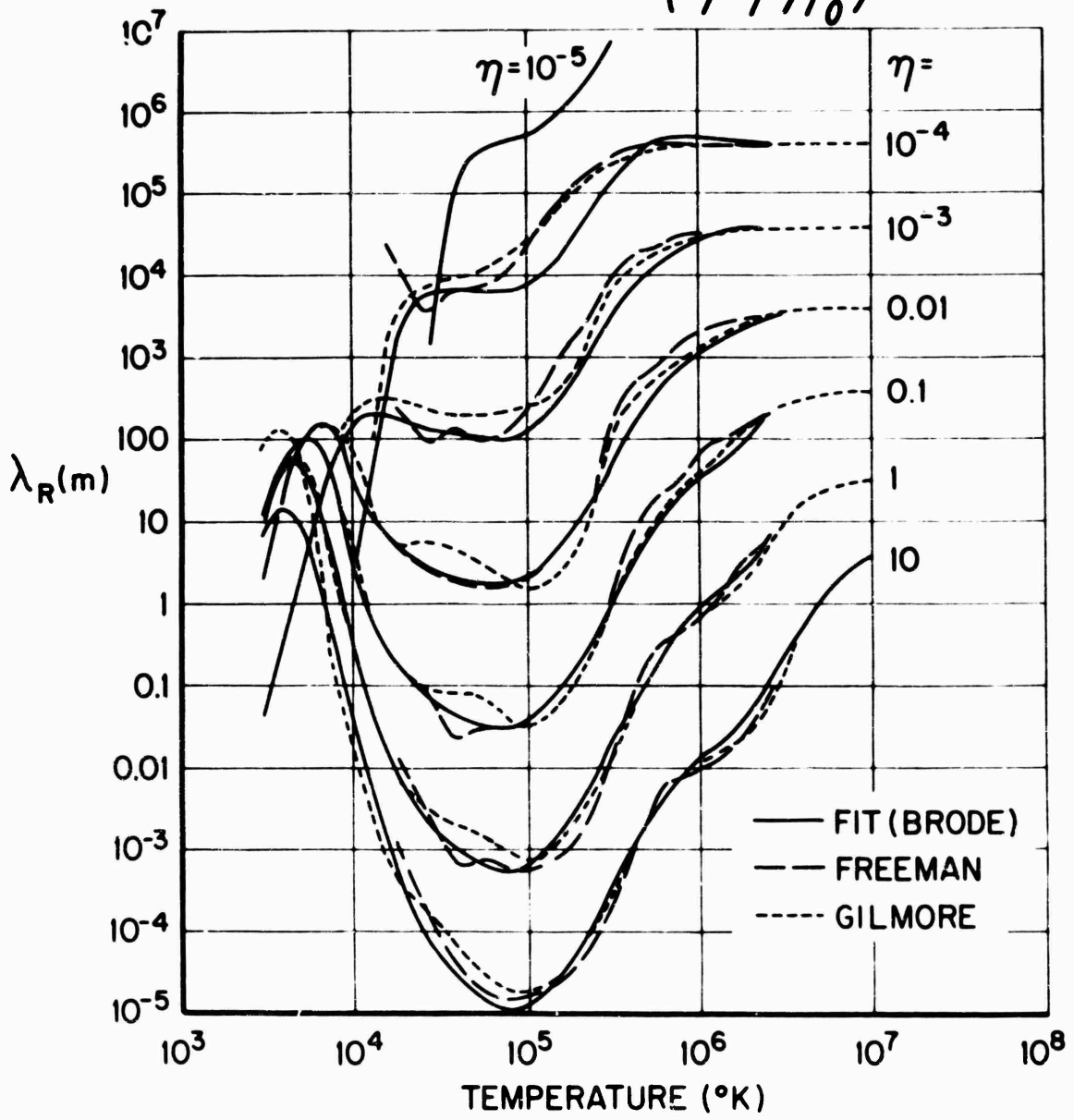

Fig. 24

ALTITUDE EFFECT ON SHOCK FORMATION—DENSITY RATIO VS REDUCED RADIUS

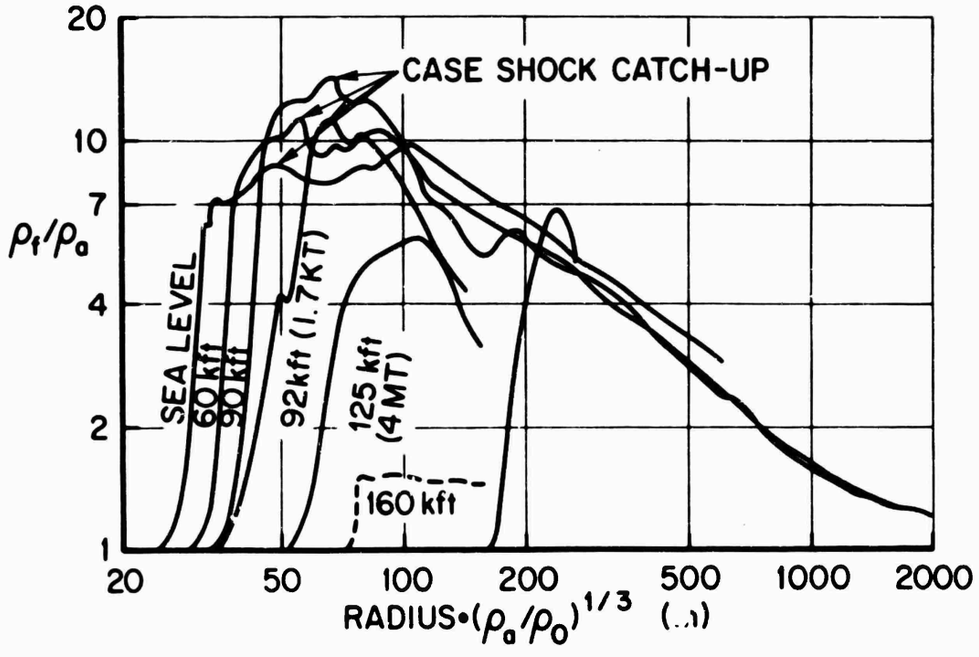

Fig. 25

cantly different, and the shock formations, if any, are late and likely to be less pronounced.

Figure 26 shows the influences of altitude on the central temperatures. Here again the scaling for the time is by the cube root of the density ratio, and the yields have been scaled to 200 kilotons. The complete failure of the similarity in these solutions is due to the difference in the radiative properties of these fireballs. The sea level case supports the highest temperature for the longest time; the higher altitudes show an inability to maintain high temperatures for the even relatively short times because of their greater transparency.

In Fig. 27 the radius-time data for these high altitude calculations are superimposed for the sake of comparisons between the various features. The radiative growth, as one goes to higher altitudes, goes to larger distances at the early times, and clearly fails to scale by this simple cube-root scaling. The case shock which should not be so sensitive to atmospheric conditions also fails to follow this scaling, but in roughly the opposite direction since this shock position should be relatively independent of the ambient density in these early phases. The extent of the expansion of the debris, although not correctly predicted by these calculations, does indicate an expected trend in that the late time debris expansion should be proportional to the mass which it has displaced and so scale appropriately by this cube root of the density. On the other hand, the late time shock is reasonably predicted by this scaling, even though the early phases fail seriously to follow the same scaling law. However, at the highest altitudes, one may be forced to wait for very long times and to very large distances before the cube root of ambient density scaling might become appropriate.

When one looks at the scaling with altitude for the radius of shock formation (or the radius at which the transition between radiative and hydrodynamic growth occurs) guided by these few calculations, the extent of the deviation from such a cube-root scaling becomes clear (Fig. 28). There is some ambiguity in what one might call the radius which is appropriate to shock formation,

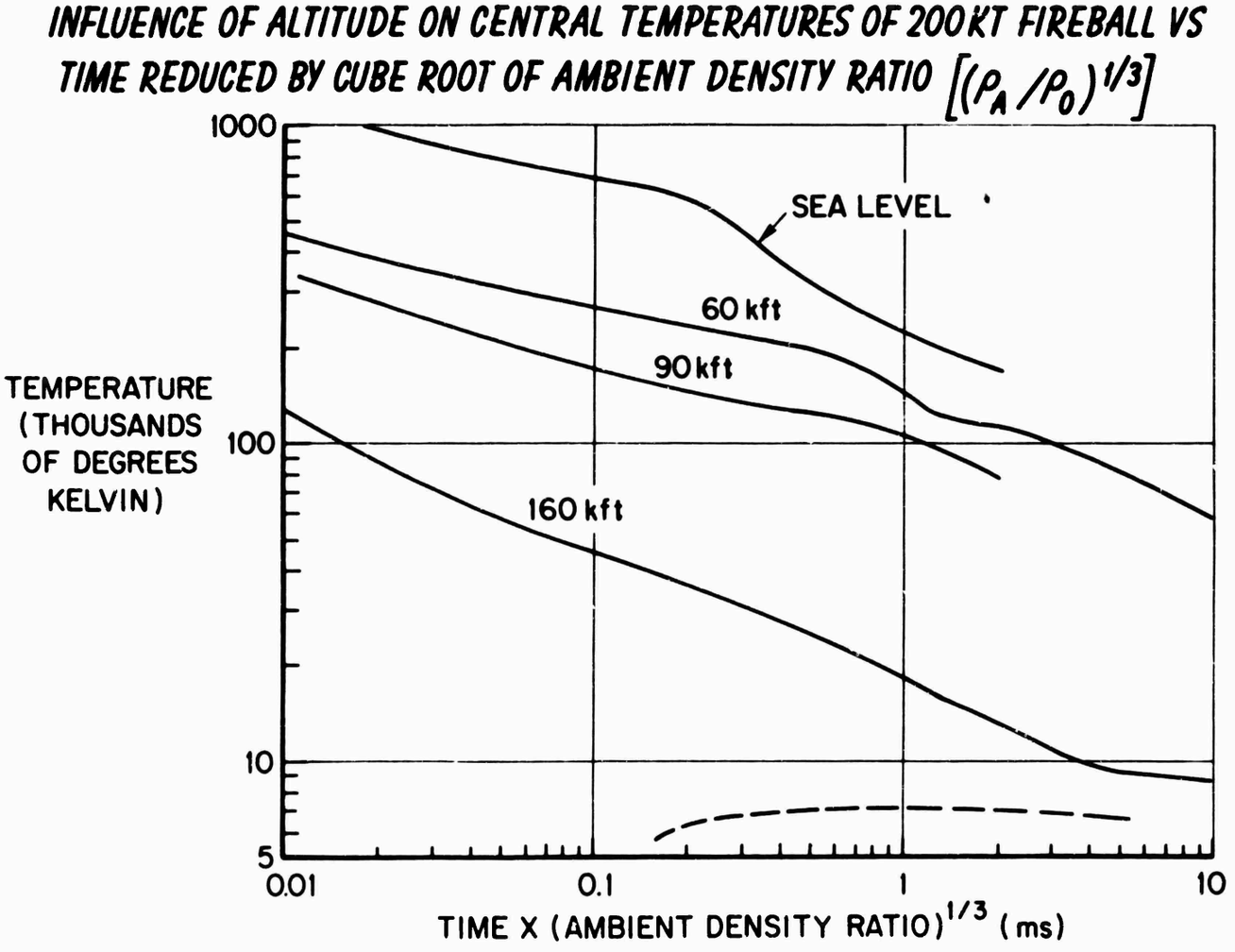
INFLUENCE OF ALTITUDE ON CENTRAL TEMPERATURES OF 200 KT FIREBALL VS TIME REDUCED BY CUBE ROOT OF AMBIENT DENSITY RATIO $[(\rho_A/\rho_0)^{1/3}]$
TEMPERATURE (THOUSANDS OF DEGREES KELVIN)
1000
100
10
5
SEA LEVEL
60 kft
90 kft
160 kft
0.01
0.1
1
10
TIME X (AMBIENT DENSITY RATIO)$^{1/3}$ (ms)

Fig. 2

ALTITUDE EFFECT ON EARLY SPACE-TIME (200 KT)

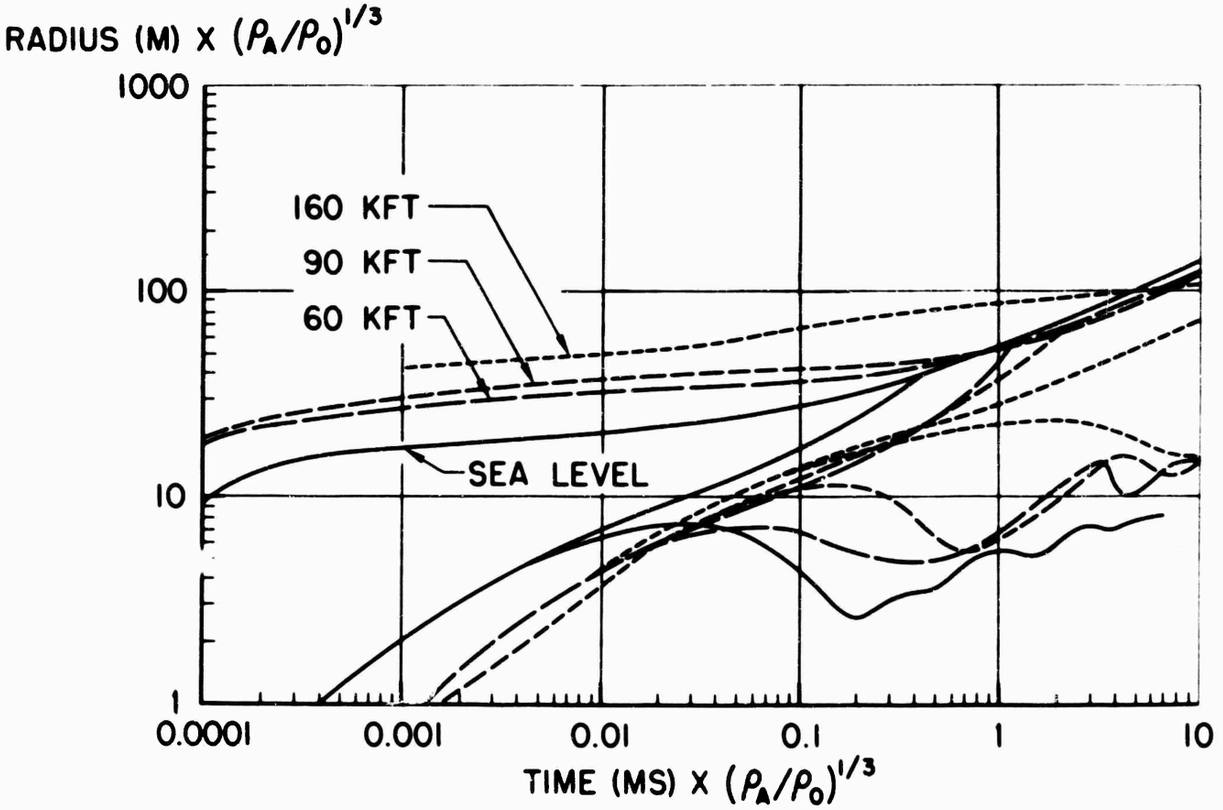

Fig. 27

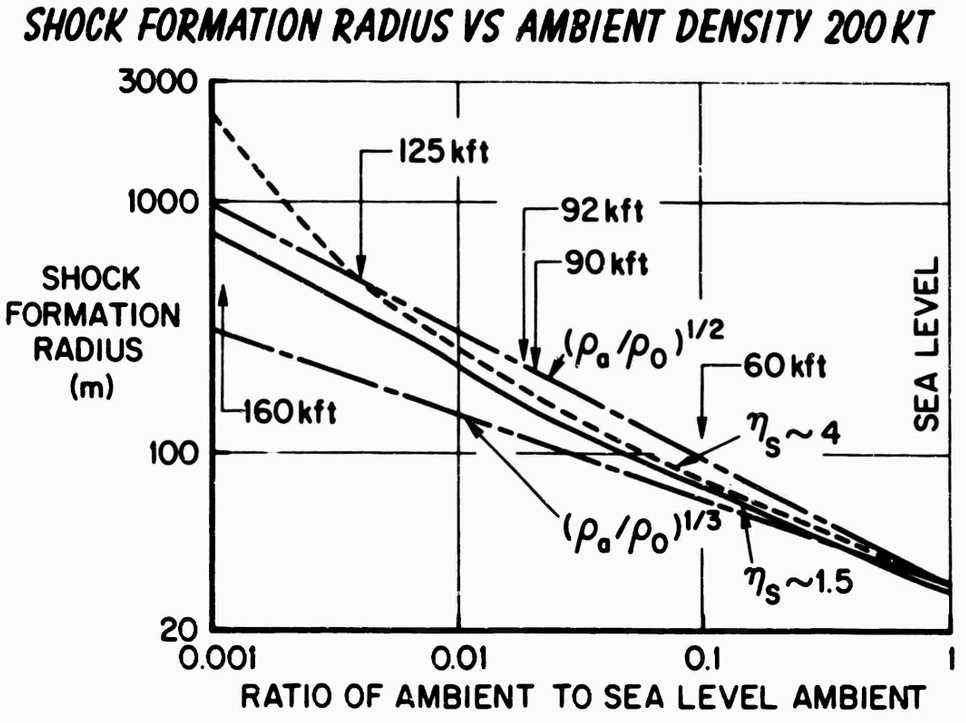
SHOCK FORMATION RADIUS VS AMBIENT DENSITY 200 KT
3000
1000
100
20
SHOCK FORMATION RADIUS (m)
125 kft
92 kft
90 kft
$(\rho_a/\rho_0)^{1/2}$
60 kft
160 kft
$\eta_s \sim 4$
SEA LEVEL
$(\rho_a/\rho_0)^{1/3}$
$\eta_s \sim 1.5$
0.001
0.01
0.1
1
RATIO OF AMBIENT TO SEA LEVEL AMBIENT

Fig. 28

that is, how much compression must there be in the shock before one considers it to be a proper adiabatic shock. Consequently, two levels of compression are plotted here. One when the density has increased by 50%, i.e., where the density is appreciably above ambient, and the other example follows the radius at which it has first reached four times the ambient density. These two curves do not follow a simple power law in the density ratio, but the 50% compression curve is more nearly amenable to a simple power law. It follows more nearly a square-root dependence on the ambient density, however, rather than the cube-root dependence. The higher compression of four times normal density requires, at higher altitudes, a relatively larger radius. It is fairly evident that the deviations are more severe at high altitudes, and at the same time the methods used here for calculations are least appropriate there. Even so, it is to be expected that such a transition would fail to scale in a simple way, but perhaps the square-root dependence on density is the most appropriate approximate scaling to apply.

Of some considerable interest beyond the fireball itself, is the amount of radiation and the timing and character of the thermal radiation which is radiated to large distances. In calculating this radiation for these approximate calculations, it is necessary to consider the effective mean free paths for emission from the air at various temperatures and densities.

Figure 29 illustrates both the approximate data as provided by Gilmore at RAND and a fit used in the calculations to model this information for the numerical work. Here the salient features are the marked dependence on density showing mean free paths which become extremely long at the higher densities and further showing that all mean free paths at all densities become very long at low temperatures. In fact, below 4000^{o} the emission mean free paths very rapidly become enormous.

Using these descriptions of emission mean free paths, one calculates the effective radiating rate as a fraction of the black-body rate coming from each element of the system which is less than black-body by the ratio of the thickness of the zone to the local value of

EMISSION MEAN FREE PATHS FOR AIR (USED IN GREY-BODY LOSS CALCULATIONS OF FIREBALL THERMAL LOSS)

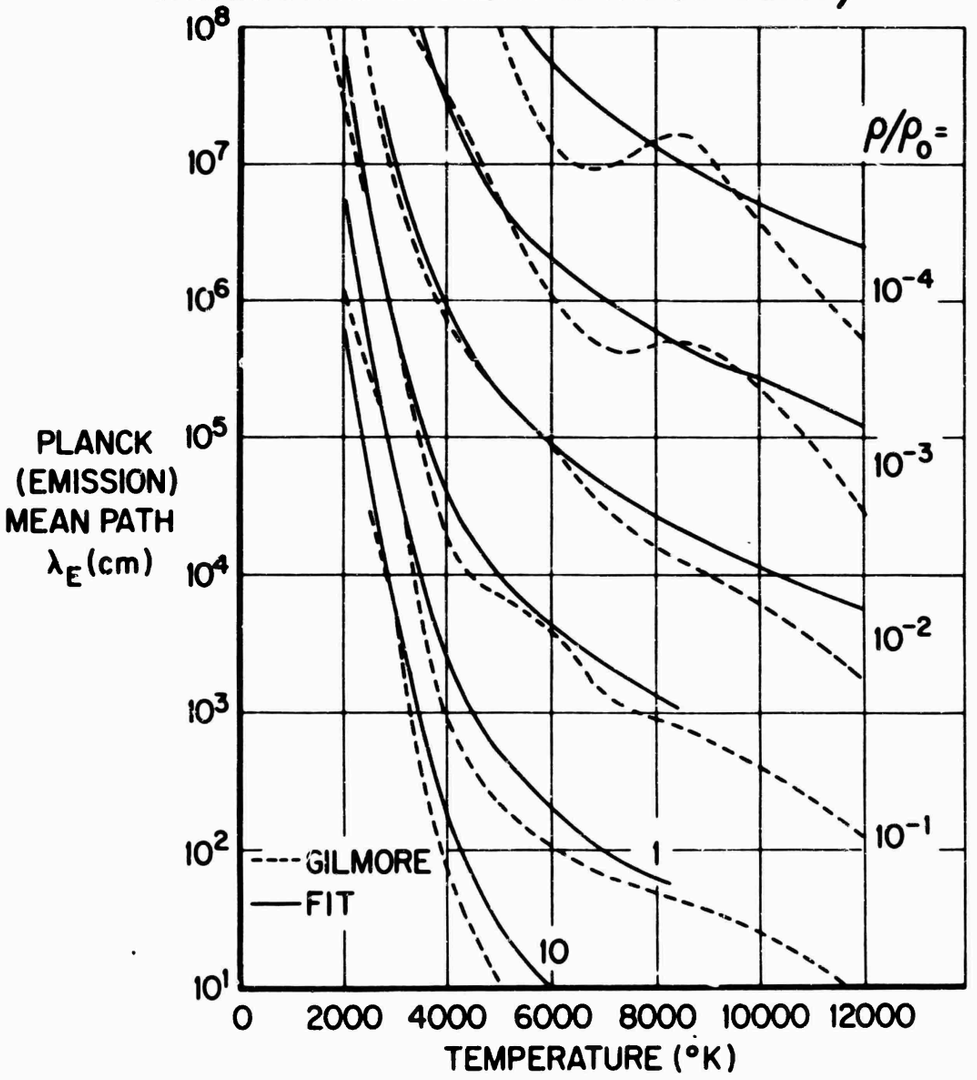

Fig. 29

the emission mean free path. That is, where the mean free path is very long compared to the thickness of some radiating zone of air, then a very small fraction of the blackbody rate is extracted from that air, extracted from the fireball or the system of hydrodynamics and radiation diffusion. Such losses are extracted from only those regions closer than one mean free path to the outer surface or shock front.

Figure 30 illustrates something of the nature of this optical depth concept in that it shows mean free paths as a function of radius for the fireball at various times shortly before and after the time of maximum thermal power output. The earliest curve at 0.12 seconds shows that mean free paths are nearly everywhere much shorter than the radius of the fireball itself. At two tenths of a second the mean free paths in the hot region are becoming comparable to the dimensions of that hot region and are already larger than the fireball radius in the cooler exterior air. At a half a second for this 200 kiloton example, mean free paths are everywhere nearly a kilometer in length, while the fireball is of radius less than a kilometer. In other words, the fireball is already nearly transparent or a fraction of a mean free path thick.

The earliest radiation, that is the radiation that comes from the fireball while the fireball front or shock front is still relatively opaque (frequently calculated as the radiation prior to minimum), is shown in Fig. 31 as approximated from these calculations. Two fractions are illustrated in per cent; the upper curve includes essentially all of the energy which is expected to leave the fireball, the lower curve being the fraction which one might expect to see at large distances after the additional absorption in the ultraviolet by oxygen and ozone in the intervening cold atmosphere.

We see, then, that because of the changing features of the fireball, the thermal radiation to be expected from a nuclear explosion changes markedly as the altitude of burst is changed.

Figure 32 indicates schematically the relative nature of three general regimes of altitudes of burst. At sea level, where the fireball is small and relatively opaque for much of its history, the rate

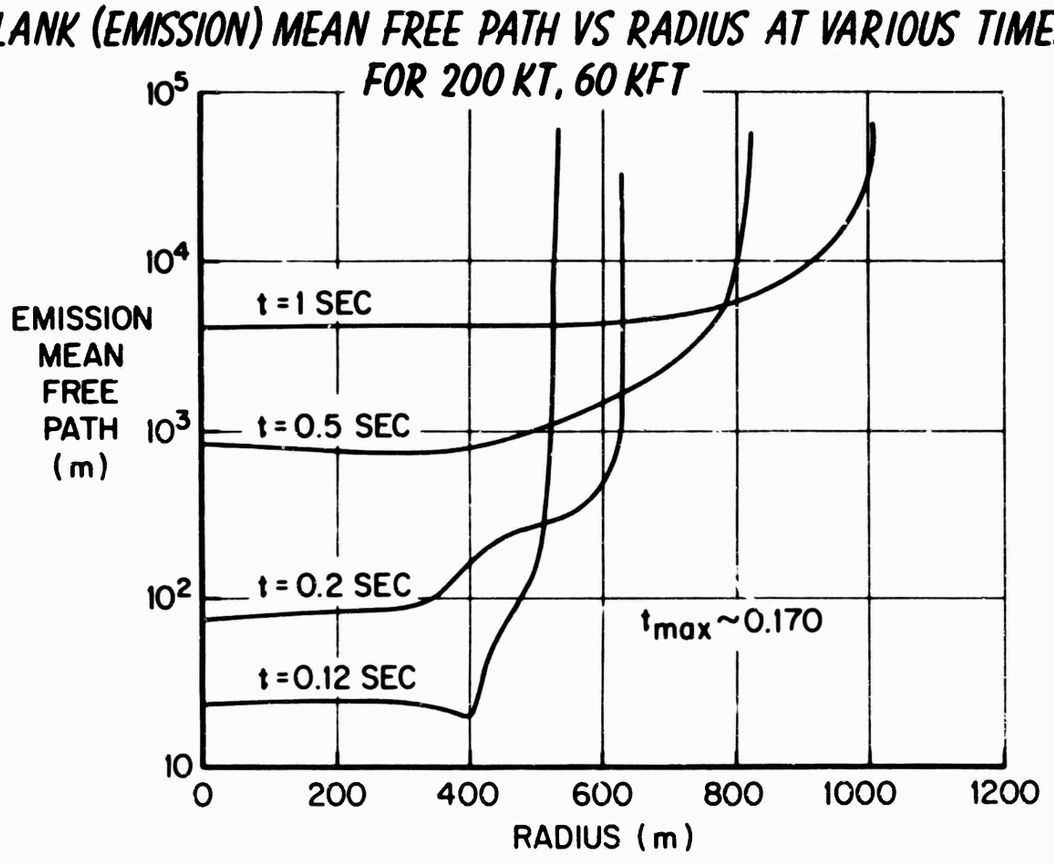
PLANK (EMISSION) MEAN FREE PATH VS RADIUS AT VARIOUS TIMES
FOR 200 KT, 60 KFT
EMISSION MEAN FREE PATH (m)
10^5
10^4
10^3
10^2
10
t = 1 SEC
t = 0.5 SEC
t = 0.2 SEC
t = 0.12 SEC
$t_{max} \sim 0.170$
0
200
400
600
800
1000
1200
RADIUS (m)

Fig. 30

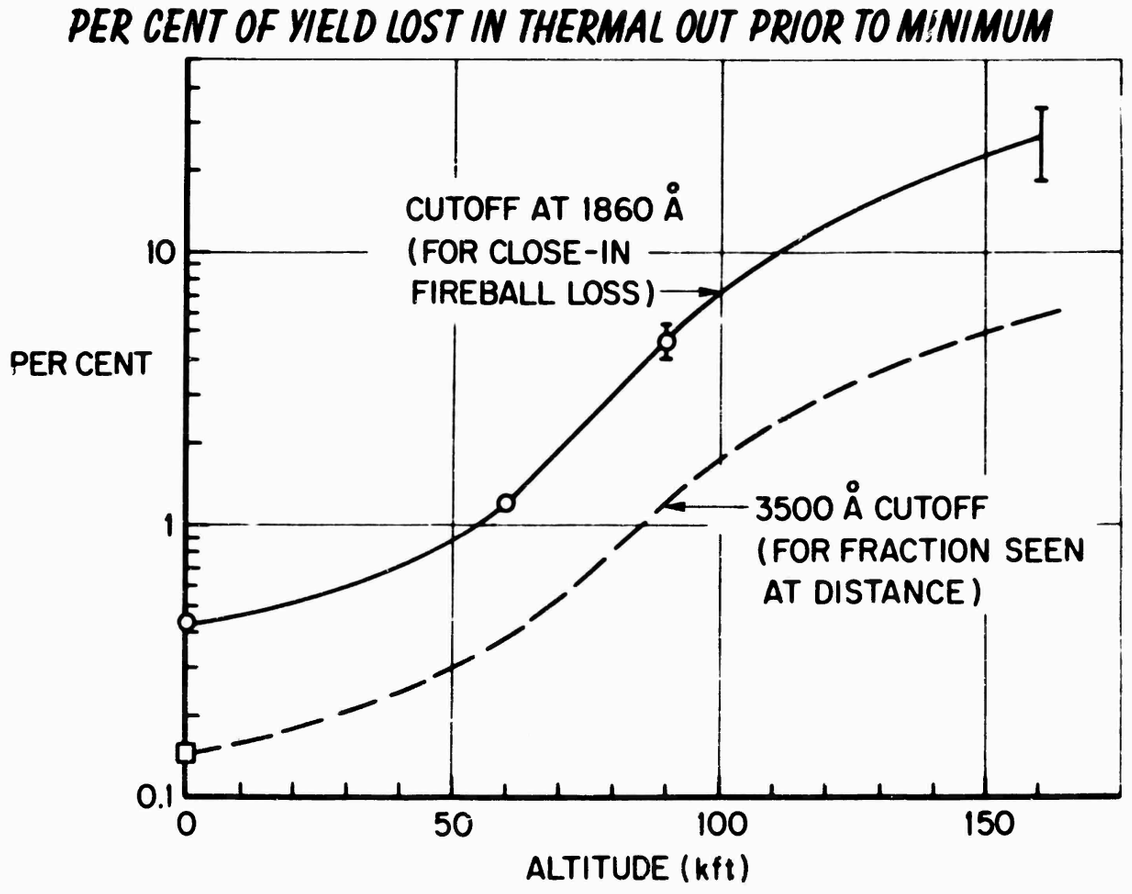
PER CENT OF YIELD LOST IN THERMAL OUT PRIOR TO MINIMUM
CUTOFF AT 1860 Å
(FOR CLOSE-IN
FIREBALL LOSS)
3500 Å CUTOFF
(FOR FRACTION SEEN
AT DISTANCE)
PER CENT
10
1
0.1
0
50
100
150
ALTITUDE (kft)

Fig. 31

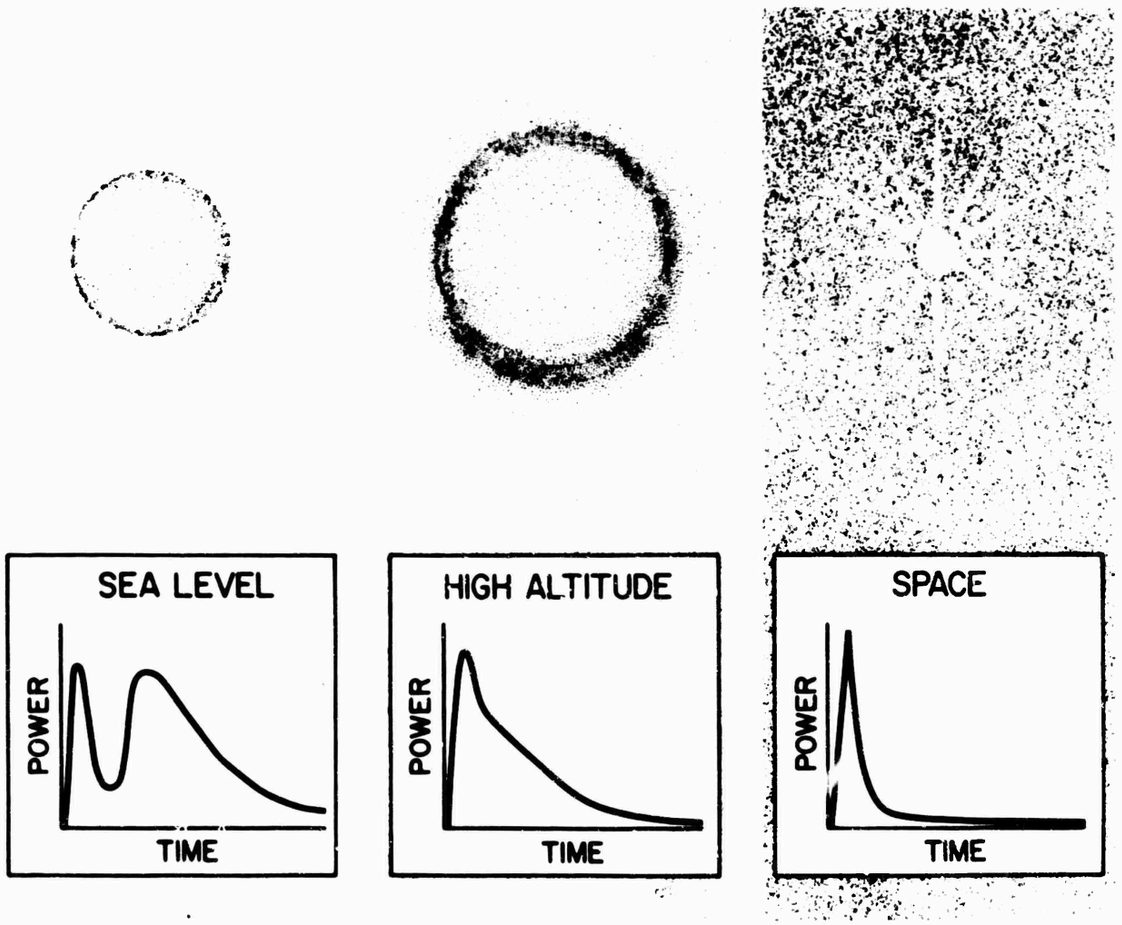

Fig. 32—Altitude effect on thermal pulse

of thermal output follows the shock growth. The eventual opening up of the fireball allows the energy in its hot interior to radiate out, giving the relatively slow, double-peaked power-time dependence. At higher altitudes, the double peak tends to disappear and the pulse tends to be faster as the fireball becomes both larger and more transparent at an earlier stage. At the very extremes of altitudes (in outer space), of course, the only visible radiations must come from the bomb vapors themselves, and will be delivered as a tail to a very high temperature spectrum in literally microseconds. In contrast, the pulse from high altitude atmospheric explosions may have durations of milliseconds, and sea level explosions may take several to tens of seconds (at megaton yields).

The relative amounts of energy lost as thermal radiation, or the total integrated power out, remains rather insensitive to altitude and very roughly is approximately the same as that which we estimate for low atmospheric or sea level explosions, that is, something of the order of one third to one half of the total yield.

In summary, then, from bursts at any altitude, one may anticipate a total amount of energy of approximately the same fraction of the yield. This energy is delivered in a time which is characterized perhaps best by an approximate scaling; proportional to the square root of the ambient density, and nearly proportional to the square root of the yield. A relatively crude scaling law then might be provided by an expression for the effective radiation time or equivalent time to maximum of about 0.044 times the square root of the density ratio times the square root of the yield in kilotons.

$$t_{max} \simeq 0.044 \sqrt{W\rho/\rho_o} \quad \text{sec}$$

This time in seconds is the approximate time-to-maximum at low altitudes, but is more like a total pulse effective time for the highest altitudes. The form is clearly not appropriate beyond 100 kilometers, and may be in serious error below that altitude for less than megaton yields.